Mayer, L., Pisias, N., Janecek, T., et al., 1992
Proceedings of the Ocean Drilling Program, Initial Reports, Vol. 138

18. SITE 853[1]

Shipboard Scientific Party[2]

HOLE 853A

Date occupied: 25 June 1991

Date departed: 25 June 1991

Time on hole: 8 hr, 4 min

Position: 7°12.661′N, 109°45.084′W

Bottom felt (rig floor; m; drill-pipe measurement): 3726.0

Distance between rig floor and sea level (m): 11.7

Water depth (drill-pipe measurement from sea level, m): 3714.3

Total depth (rig floor; m): 3735.5

Penetration (m): 9.5

Number of cores (including cores with no recovery): 1

Total length of cored section (m): 9.5

Total core recovered (m): 10.15

Core recovery (%): 106.8

Oldest sediment cored:
Depth (mbsf): 9.50
Nature: clayey nannofossil foraminifer ooze
Earliest age: late Pliocene

HOLE 853B

Date occupied: 25 June 1991

Date departed: 26 June 1991

Time on hole: 10 hr, 2 min

Position: 7°12.661′N, 109°45.084′W

Bottom felt (rig floor; m; drill-pipe measurement): 3727.2

Distance between rig floor and sea level (m): 11.7

Water depth (drill-pipe measurement from sea level, m): 3715.5

Total depth (rig floor; m): 3799.6

Penetration (m): 72.4

Number of cores (including cores with no recovery): 9

Total length of cored section (m): 72.4

Total core recovered (m): 77.68

Core recovery (%): 107.3

Oldest sediment cored:
Depth (mbsf): 72.4
Nature: nannofossil ooze with clay
Earliest age: late Miocene

[1]Mayer, L., Pisias, N., Janecek, T., et al., 1992. *Proc. ODP, Init. Repts.,* 138: College Station, TX (Ocean Drilling Program).
[2]Shipboard Scientific Party is as given in the list of participants preceding the contents.

HOLE 853C

Date occupied: 26 June 1991

Date departed: 26 June 1991

Time on hole: 8 hr, 45 min

Position: 7°12.650′N, 109°45.078′W

Bottom felt (rig floor; m; drill-pipe measurement): 3726.5

Distance between rig floor and sea level (m): 11.7

Water depth (drill-pipe measurement from sea level, m): 3714.8

Total depth (rig floor; m): 3794.7

Penetration (m): 68.2

Number of cores (including cores with no recovery): 8

Total length of cored section (m): 68.2

Total core recovered (m): 69.57

Core recovery (%): 102.0

Oldest sediment cored:
Depth (mbsf): 68.20
Nature: nannofossil ooze with clay
Earliest age: late Miocene

HOLE 853D

Date occupied: 26 June 1991

Date departed: 26 June 1991

Time on hole: 7 hr, 20 min

Position: 7°12.651′N, 109°45.074′W

Bottom felt (rig floor; m; drill-pipe measurement): 3724.2

Distance between rig floor and sea level (m): 11.7

Water depth (drill-pipe measurement from sea level, m): 3712.5

Total depth (rig floor; m): 3790.0

Penetration (m): 65.8

Number of cores (including cores with no recovery): 7

Total length of cored section (m): 65.8

Total core recovered (m): 68.81

Core recovery (%): 104.6

Oldest sediment cored:
Depth (mbsf): 65.8
Nature: nannofossil ooze with clay
Earliest age: late Miocene

HOLE 853E

Date occupied: 26 June 1991

Date departed: 26 June 1991

Time on hole: 8 hr, 30 min

Position: 7°12.651′N, 109°45.074′W

Bottom felt (rig floor; m; drill-pipe measurement): 3725.2

Distance between rig floor and sea level (m): 11.7

Water depth (drill-pipe measurement from sea level, m): 3713.5

Total depth (rig floor; m): 3743.2

Penetration (m): 18.0

Number of cores (including cores with no recovery): 2

Total length of cored section (m): 18.0

Total core recovered (m): 18.51

Core recovery (%): 102.8

Oldest sediment cored:
Depth (mbsf): 18.0
Nature: nannofossil foraminifer clay
Earliest age: late Pliocene

Principal results: Site 853 is the sixth of our seven-site north–south transect along 110°W. The site is located in the eastward-flowing North Equatorial Countercurrent. The objective of drilling at this site is to provide a record of the late Neogene history of this current as well as a record of accumulation resulting from transport of eolian sediments in the Northern Hemisphere trade winds.

Five holes were drilled at Site 853: Hole 853A, a single APC mud-line core dedicated to whole-round geochemical and physical property measurements; Hole 853B, APC-cored to 72.4 mbsf before the final core struck what we assumed was basement, and the core cutter in the last core was destroyed during recovery of basalt; Hole 853C, APC-cored to 66 mbsf and one XCB core drilled to basement; Hole 853D, APC-cored to 68.8 mbsf; and finally, two APC cores were retrieved in Hole 853E to sample an interval where the collapse of a core liner in a previous hole resulted in a damaged section and some uncertainty when constructing a complete composite section.

Bad weather during drilling operations caused significant swells and for the first time during Leg 138, we found it difficult to control the overlap in adjacent APC-cored holes. Even with the number of holes drilled, a short gap is present in the section and for the first time since Site 844, an interval was re-cored by successive APC cores. Thus, even having a large heave compensator, such as that on the *JOIDES Resolution,* ship's motion can result in difficulties in recovering continuous records for paleoceanographic study.

Sediments in the 73-m section of Site 853 are dominated by calcareous microfossils with minor amounts of clay, foraminifers, and oxides. Siliceous microfossils are present in minor amounts in the upper few meters and are rare or absent throughout the rest of the sequence.

Stable magnetic remanence was measured throughout the entire section of Site 853 and with the exception of three short intervals, we were able to define polarity direction. We were also able to correlate the magnetic reversal pattern to the magnetic polarity time scale for all events from Chron C4A through the Brunhes.

A well-constrained biostratigraphy was obtained primarily from calcareous nannofossils. Comparison of the paleomagnetic and nannofossil stratigraphies provides new biochronologic data for calibration of nannofossil events. Foraminifers are poorly preserved and are abundant only in the Pleistocene and Pliocene. Radiolarians and diatoms are rare and poorly preserved in the younger interval and present as scattered fragments in the Miocene.

Sedimentation rates, based on excellent paleomagnetic results at Site 853, are ~15 m/m.y. in the late Miocene, decrease to ~8 m/m.y. in the Pliocene, and to 4 or 5 m/m.y. in the Pleistocene. Superimposed on this general decrease in sedimentation rates are short intervals of increased sedimentation rates in the latest Miocene and early Pliocene that are similar in pattern to changes seen at other sites drilled during Leg 138. Overall reduced sedimentation rates throughout the history of Site 853 and the marked reduction in siliceous microfossils are consistent with the reduced productivity associated with the more northerly position of the site.

While the paleoceanographic placer thins for the diatoms and radiolarians, the excellent magnetic and nannofossil stratigraphy will make Site 853 a unique record for studying eolian sedimentation associated with the Northern Hemisphere trades. At the conclusion of Site 853, Leg 138 paleomagnetists had completed 8.98 log(m^2kt).

BACKGROUND AND SCIENTIFIC OBJECTIVES

Site 853, near the northern end of our seven-site 110°W transect, is located in the eastward flowing North Equatorial Countercurrent (NECC; Fig. 1). The objective of drilling at this site is to provide a record of the late Neogene history of this current as well as a record of terrigenous accumulation resulting from transport in the Northern Hemisphere trade winds. Sediments collected at this site will contain the first equatorial Pacific Ocean record of a relatively long history of eolian transport, a key indicator of the history of atmospheric circulation.

Site 853 is located on crust formed at the East Pacific Rise (Fig. 2) and, based on basement subsidence and estimates of spreading rate for this sector of the Pacific Ocean, the basement age at Site 853 was expected to be ~13 Ma. A detailed survey of the region that surrounds the site was conducted as part of the *Thomas Washington* Venture 1 cruise. The north–south-trending topography of this site has a total relief of almost 400 m (Fig. 3) and most likely reflects original ridge crest structure. The sediment cover in this region is variable, with sediment accumulating on local highs and in troughs and virtually no accumulation on the intervening slopes. This pattern of sediment distribution is probably typical of areas with low sedimentation rates and topographically enhanced bottom current activity. Site 853 is located on top of a small regional high and thus has probably been protected from bottom current activity. The seismic section (Fig. 4) shows an ~65-m-thick sedimentary section at the proposed site.

OPERATIONS

Transit to Site 853

The transit from Site 852 to Site 853 (proposed Site WEQ-7) covered 104 nmi at an average speed of 11.4 kt. At 0245L (all times reported in operations text are local time, L, where L = Universal Time Coordinated, UTC – 7 hr; all times in Table 1 are UTC) 25 June, the vessel slowed to 6 kt as we deployed seismic equipment for a short survey. At 0419L, an acoustic beacon was launched successfully on location and the survey continued for 10 min past the site. The survey covered 13.5 nmi at an average speed of 5.9 kt. At the end of the survey, the water guns were retrieved and the ship returned to the site location. The hydrophones and thrusters were lowered and in place by 0530L 25 June. The depth to seafloor, based upon the precision depth recorder, was 3726.4 m below rig floor (mbrf).

Hole 853A

This hole was dedicated to whole-round samples for geochemical and physical property studies. The drill pipe was lowered to 3720 mbrf where the first piston core was taken at 1130 hr, 25 June. The core barrel was retrieved empty (water core) but mud found on the cutting shoe indicated contact with the seafloor.

The next piston core was taken 6 m lower. A full core barrel was retrieved (10.15 m) and the mud line was inferred to be 3726 mbrf (see Table 1 for a summary of coring operations).

Hole 853B

The mud-line core for this hole was taken in a water depth of 3722 m at 1340L 25 June. The advance intervals for Cores 138-853B-2H, -3H, and -4H were reduced to 8 m in an attempt to study the effects of core expansion. The normal piston coring interval of 9.5 m was resumed with Core 138-853B-5H, when the results of the core expan-

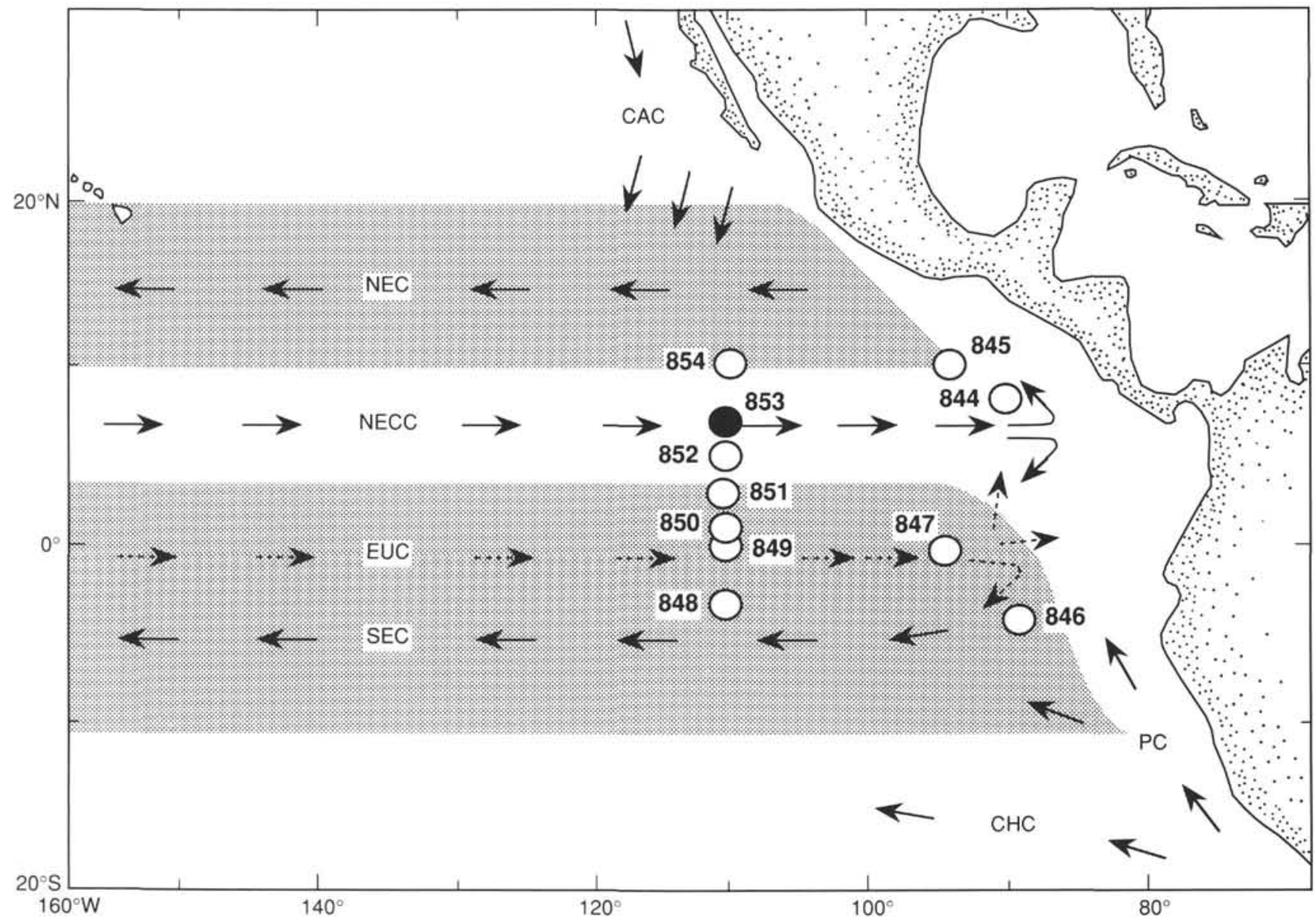

Figure 1. Location of Site 853 and generalized circulation system of the eastern equatorial Pacific Ocean. The other Leg 138 sites are shown for reference. Surface current shown as solid arrows, sub-surface current as dashed arrows. CAC = California Current; NEC = North Equatorial Current; NECC = North Equatorial Countercurrent; EUC = Equatorial Undercurrent; SEC = South Equatorial Current; PC = Peru Current; CHC = Chile Current. Shaded area illustrates general latitudinal extent of the SEC and NEC.

sion exercise were inconclusive. In this hole, multishot orientation began with Core 138-853B-5H. Coring ended in this hole when Core 138-853B-9H hit basement at 72.4 mbsf; recovery was 107.3%. The inflated recovery figure resulted from the recovery of full core barrels (over 9.5 m) in Cores 138-853B-2H through -4H, which were advanced only 8.0 m. After Core 138-853B-9H was retrieved, the pipe was pulled out of the hole and the bit cleared the seafloor at 2225L 25 June, ending Hole 853B.

Hole 853C

The ship was offset 20 m south, the bit lowered to 3726 mbrf and the mud-line core taken at 2330L 25 June. Piston coring advanced to a depth of 66.0 mbsf (Core 138-853C-7H), with multishot orientation starting with Core 138-853C-4H. The XCB-coring system was used with the eighth core in an attempt to retrieve the sediment/basement contact. The core barrel effortlessly advanced 2.2 m when a sudden decrease in rate of penetration and an increase in torque indicated basement contact. Time constraints did not allow for coring into basement and the core barrel (Core 138-853C-8H) was retrieved with 1.27 m of sediment. The recovery was 103.5% for the APC-cored section and 57.7% for the XCB-cored section.

Once the last core was on deck, the pipe was pulled out of the hole and the bit cleared the seafloor at 0710L 26 June, ending Hole 853C.

Hole 853D

This hole was drilled to ensure that a continuous sequence was recovered and enough material was available for high-resolution sampling. The vessel was offset 20 m east and the pipe lowered to 3723 mbrf. Core 138-853D-1H was retrieved at 0820L June 26, and from it, we recovered 8.81 m of sediment. Piston-coring advanced through Core 138-853D-7H, which stopped just short of basement. Cores were oriented starting with Core 138-853D-4H. Recovery in this hole was 104.6%. After the last core barrel was recovered, the pipe was pulled out of the hole, and the bit cleared the seafloor at 1430L 26 June, ending Hole 853D.

Hole 853E

This hole was drilled to sample an interval where liner collapse in a previous hole resulted in a damaged section. The vessel was offset 20 m south and Core 138-853D-1H was retrieved at 1530L 26 June. Because of time constraints, only one additional core was recovered. Recovery in this hole was 102.8%.

After we retrieved the last core, and as the pipe was pulled out of the hole, a beacon was released by remote command and was back on deck at 1827L 26 June. The bit was on deck by 2235L 26 June, after which the rig floor was secured, and the thrusters and hydrophones were raised. The ship began the transit to Site 854 at 2300L 26 June.

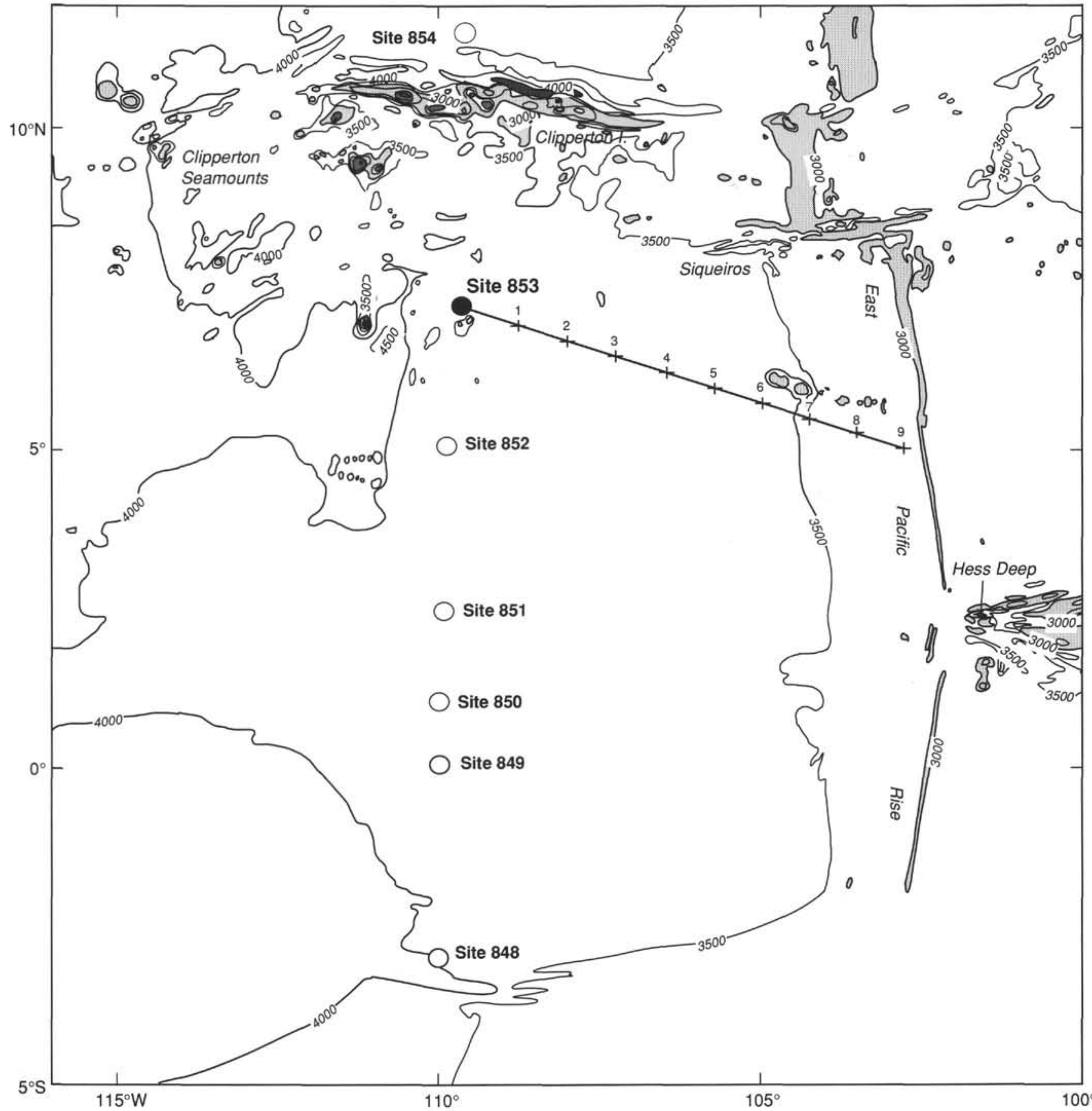

Figure 2. Generalized bathymetric map showing location of Site 853 and other Leg 138 sites drilled along the 110°W transect (From Mammerickx, 1989). Backtrack path (using the pole of rotation of van Andel et al., 1975) shown for 1 m.y. increments. Bathymetry in meters.

LITHOSTRATIGRAPHY

Introduction

A 72.4-m sequence of Pleistocene to upper Miocene sediments was recovered from the five holes drilled at Site 853. Hole 853A consists of a single core that was dedicated to pore-water and physical properties sampling. Holes 853B, 853C, and 853D provide nearly continuous recovery of the sedimentary column. Hole 853E was cored to provide additional recovery and ensure overlap in the upper portion of the sedimentary sequence. Several basalt fragments were present within Core 138-853B-9H. The sediment below the uppermost basalt fragment in Section 2 at 35 cm is similar to material higher in the sedimentary section and probably represents re-cored sediment that was recovered when the APC rebounded after striking basement. Hole 853C was APC-cored to 66 mbsf and XCB-cored to basement at 68.2 mbsf. Hole 853C is lithologically similar to Hole 853B above the first basalt fragment in Hole 853B but does not contain the additional material recovered below it, reaffirming our suspicion that sediment below 68.15 mbsf in Hole 853B represents re-cored material.

The following lithologic description (summarized in Fig. 5) is based on visual core descriptions, smear slide estimates of sedimen-

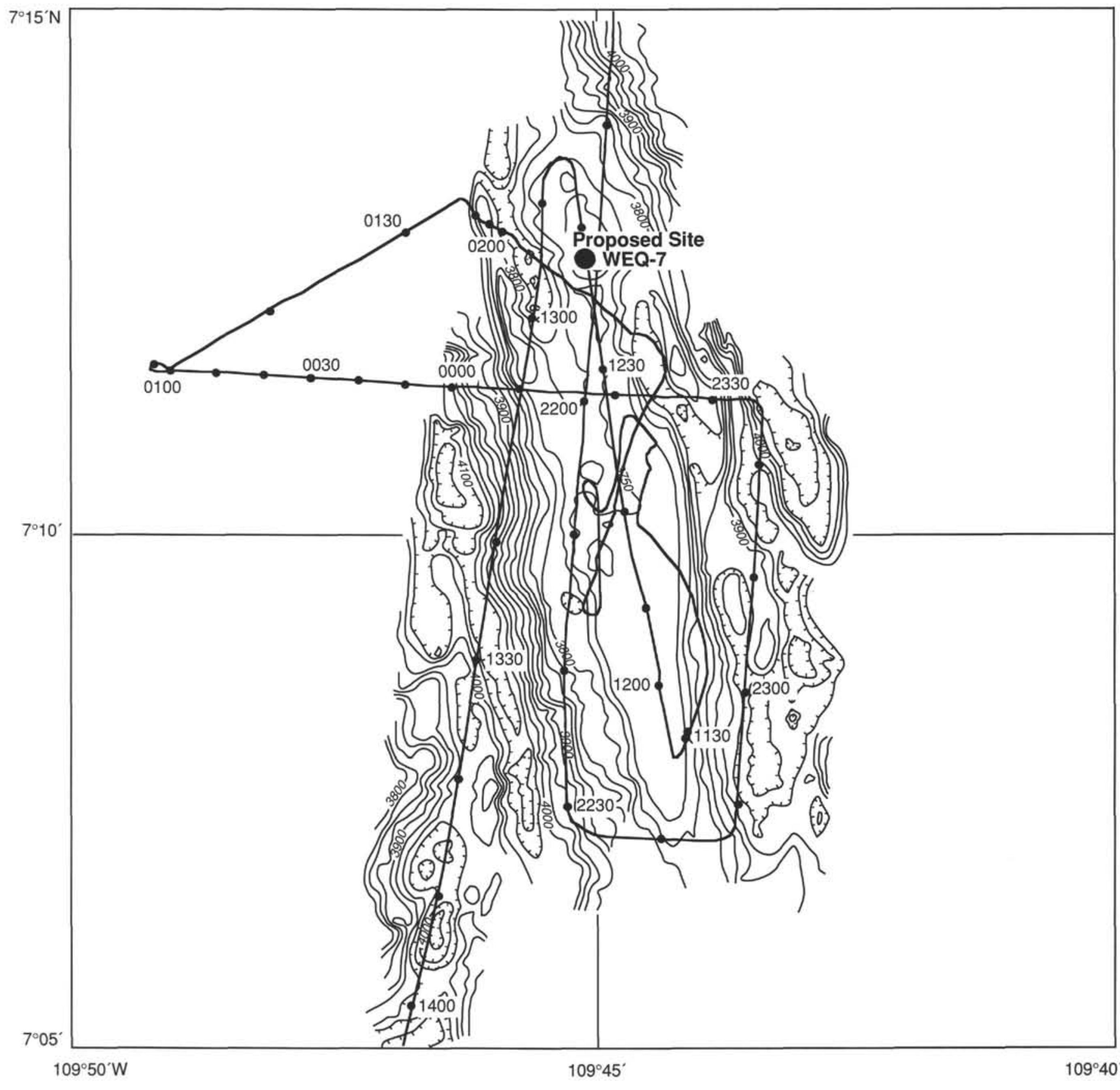

Figure 3. SeaBeam map hand-contoured from navigation-adjusted SeaBeam contour maps collected on the *Thomas Washington* during Venture 1 cruise, September 1989. Proposed Site WEQ-7 is shown.

tary components, and continuously measured lithologic parameters (GRAPE bulk density, magnetic susceptibility, and color reflectance spectroscopy, Fig. 6). The results of physical property and sediment chemistry measurements were also considered.

Sediments from Site 853 are dominated by nannofossils and contain variable amounts of clay, foraminifers, and oxides. Siliceous microfossils are present in minor amounts in the upper few meters and rare to absent throughout the entire sequence below (Fig. 7). Sediments are generally very pale brown (10YR 8/2) to dark brown (10YR 2/2), reflecting variations in both the oxide and clay content. Light gray (5Y 7/1) to white (N8) colors also occur between 35–39, 44–48, and 56–66 mbsf where nannofossils comprise virtually the entire sedimentary component.

Description of Units

Lithologic Unit I

Intervals:
Core 138-853A-1H
Cores 138-853B-1H through -9H
Cores 138-853C-1H through -8X
Cores 138-853D-1H through -7H

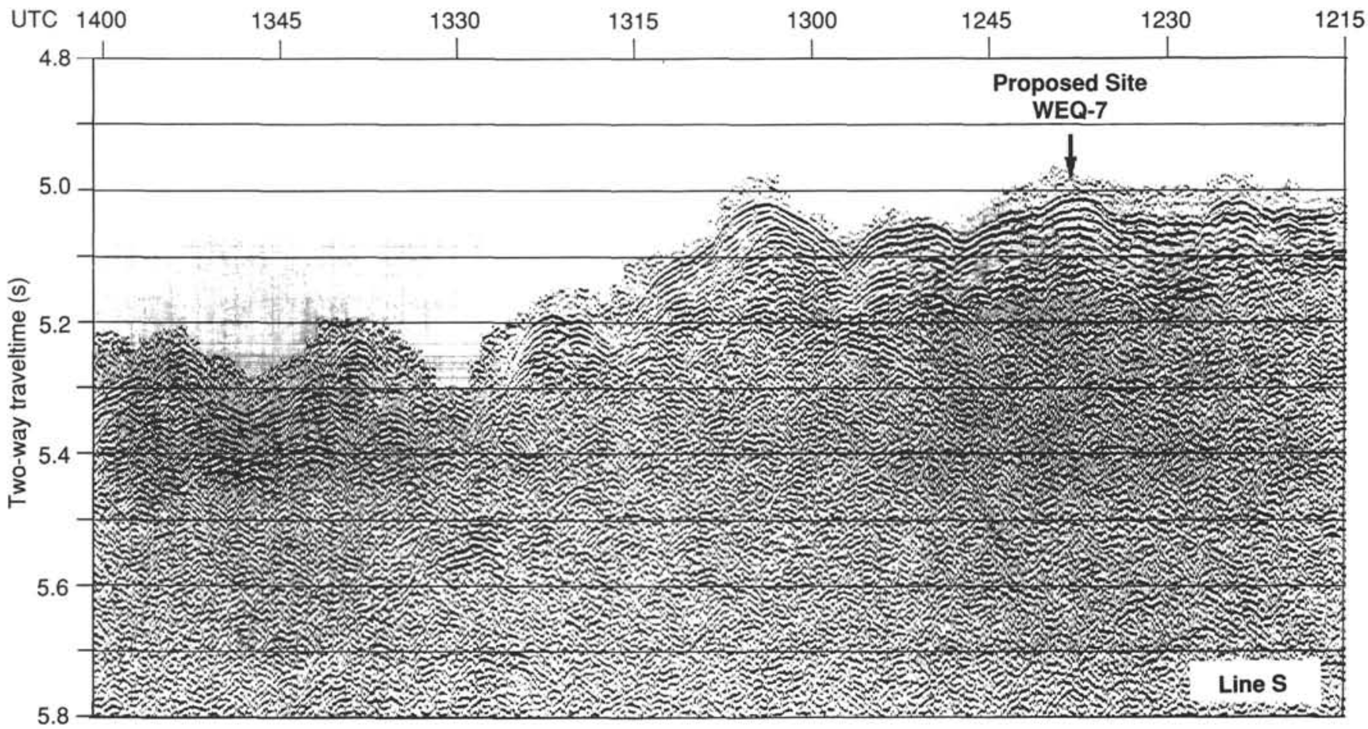

Figure 4. Analog seismic line collected with an 80-in.^{3} water gun during the *Thomas Washington* Venture 1 cruise. Proposed site WEQ-7 is shown.

Cores 138-853E-1H through -2H
Age: Pleistocene to late Miocene
Depth: 0–9.5 mbsf, Hole 853A; 0–72.4 mbsf, Hole 853B; 0–68.2 mbsf, Hole 853C; 0–65.8 mbsf, Hole 853D; 0–18.0 mbsf, Hole 853E

The upper 28 m of sediment at Site 853 is Pleistocene to lower Pliocene clayey nannofossil foraminifer ooze and foraminifer clayey nannofossil ooze. Sediment color in this upper interval is characterized by darker brown hues of 10YR 5/3–10YR 2/2 and has low percent reflectance (Fig 8). Iron and manganese oxides are abundant in this interval and their variations appear to be the primary cause for variations in color.

Foraminifer content is greatest from 0 to 12 mbsf and decreases from 50%–60% to <10% near 28 mbsf (Fig. 7). The proportion of clay component is variable throughout the upper 28 m but generally ranges between 10% and 20%. Sediments between 13 and 23 mbsf are lower in %$CaCO_3$ (see "Inorganic Geochemistry" section, this chapter) and contain several intervals in which clay is the dominant lithologic component. These intervals are characterized as dark yellowish brown to very dark brown (10YR 3/6–10YR 2/2) nannofossil clay and contain up to 15% iron and manganese oxides.

The sediments below ~28 mbsf are predominantly nannofossil ooze and contain variable amounts of clay. Foraminifer abundance is low throughout this interval (generally <10%). Clay percentages are slightly lower than in the upper portion (10%–15%); however, fewer clay-rich intervals are found in these sediments. Munsell colors are much paler than those in the uppermost interval and vary between yellowish-brown and pale brown (10YR 5/4–10YR 8/2).

Several intervals from the lower part of Site 853 show an abrupt change in lithology and contain almost 90% nannofossils. The most distinct interbeds, found between 35–39 mbsf, 44–48 mbsf, and 56–66 mbsf, also are marked by a sudden change from oxidized colors (pale brown to brown) to reduced colors (light gray to white). Continuously measured lithologic parameters clearly distinguish these layers, which have high densities, low susceptibility, and high visible reflectance (Fig. 6). Because most of the sediments from Site 853 have two principle components (clay and carbonate), the GRAPE bulk density and susceptibility measurements vary inversely to each other (Fig. 6). Higher GRAPE values are associated with a greater proportion of carbonate component.

Below ~50 mbsf, in Cores 138-853B-7H to -8H, 138-853C-6H to -7H, and 138-853D-6H to -7H, gray (10YR 6/1) and yellow (2.5Y 7/6) manganese-rich bands occur. Also present below ~60 mbsf are manganese-oxide dendrites and a number of small pods of hematite, which result in relatively high susceptibility values in the basal sediments. GRAPE density values remain consistently high and reflect the high percentage of nannofossils in the lower sediments. Basalt fragments were recovered in Section 138-853B-9H-2, 35 cm.

Color Reflectance Spectroscopy

The digital color reflectance data from Site 853 (Fig. 8) are dominated by oxidized sediments. The upper 32 m of the sedimentary column has relatively low visible reflectance, but high near-infrared reflectance. This low visible reflectance indicates the presence of oxides and clay diluting carbonate sediments. Below ~34 mbsf, reflectance of the clayey nannofossil ooze is much higher, but variable. A short interval from ~44 to 48 mbsf contains sulfides, and has relatively high reflectance in the visible bands. This zone, illustrated by a color reflectance spectrum from Section 138-853B-6H-6, 10 cm (46.40 mbsf) in Figure 8, has reflectance in the near infrared bands of ~60%, similar to that in adjacent oxidized sediments. Oxidized sediments resume below 48 mbsf, with highly variable reflectance. An example reflectance spectrum from Section 138-853B-8H-7, 5 cm (65.85 mbsf) has relatively high reflectance in the yellow (~600 nm) band. In this zone manganese oxides and clay are present. Low reflectance below ~72 mbsf is probably related to abundant hy-

Table 1. Summary of coring operations for Site 853.

Core	Date (June 1991)	Time (UTC)	Depth (mbsf)	Length cored (m)	Length recovered (m)	Recovery (%)
138-853A						
1H	25	1945	0–9.5	9.5	10.15	106.8
Coring totals				9.5	10.15	106.8
138-854A						
1H	25	2040	0.0–4.3	4.3	4.25	98.8
2H	25	2130	4.3–12.3	8.0	9.81	122.0
3H	25	2230	12.3–20.3	8.0	9.30	116.0
4H	25	2320	20.3–28.3	8.0	8.59	107.3
5H	25	0025	28.3–37.8	9.5	9.87	104.0
6H	25	0125	37.8–47.3	9.5	9.73	102.0
7H	25	0220	47.3–56.8	9.5	9.96	105.0
8H	25	0320	56.8–66.3	9.5	10.00	105.2
9H	25	0425	66.3–72.4	6.1	6.17	101.0
Coring totals				72.4	77.68	107.3
138-854C						
1H	26	0630	0.0–9.0	9.0	9.06	100.0
2H	26	0725	9.0–18.5	9.5	10.07	106.0
3H	26	0825	18.5–28.0	9.5	9.93	104.0
4H	26	0930	28.0–37.5	9.5	9.51	100.0
5H	26	1030	37.5–47.0	9.5	10.03	105.6
6H	26	1130	47.0–56.5	9.5	9.60	101.0
7H	26	1230	56.5–66.0	9.5	10.10	106.3
8X	26	1345	66.0–68.2	2.2	1.27	57.7
Coring totals				68.2	69.57	102.0
138-854D						
1H	26	1520	0.0–8.8	8.8	8.81	100.0
2H	26	1610	8.8–18.3	9.5	9.78	103.0
3H	26	1700	18.3–27.8	9.5	10.04	105.7
4H	26	1800	27.8–37.3	9.5	10.05	105.8
5H	26	1855	37.3–46.8	9.5	10.02	105.5
6H	26	1955	46.8–56.3	9.5	10.06	105.9
7H	26	2055	56.3–65.8	9.5	10.05	105.8
Coring totals				65.8	68.81	104.6
138-854E						
1H	26	2230	0.0–8.5	8.5	8.48	99.7
2H	26	2325	8.5–18.0	9.5	10.03	105.6
Coring totals				18.0	18.51	102.8

drothermal oxides. No smear slides were examined in this interval, but high magnetic susceptibility in this zone (Fig. 6) is consistent with this inference.

Trace Fossils

Bioturbation intensity at Site 853 is moderate within the top 10 m, strong from ~10 to 44 mbsf and more variable in the lower section. Within the top 10 m, solid burrows and rind burrows are most common. Burrowing is particularly intense between 15 and 20 mbsf where *Chondrites* and *Zoophycos* also are common. Bioturbation varies below 28 mbsf with solid burrows, *Skolithos, Planolites,* and *Zoophycos* common to abundant in the darker, clay-rich interval (Figs. 9 and 10). In the paler, nannofossil ooze and clayey nannofossil ooze between 34–39 mbsf, 44–48 mbsf, and 56–66 mbsf, only slight bioturbation is evident. The intensity of bioturbation, particularly in the upper interval at Site 853 evidences widespread deeper burrowing.

Summary

Sediments recovered from Site 853 provide a nearly continuous Pleistocene through upper Miocene depositional sequence. The uppermost 28 m contains foraminifer to clayey nannofossil oozes and has significant iron and manganese oxide content. Siliceous microfossils are present only in the upper few meters and rare to absent throughout most of the sequence below. In general, clay content varies inversely to carbonate content and comprises between 10% and 20% of the sediments although smaller interbeds of clay-rich nannofossil oozes are present.

Below 28 mbsf, sediments vary between clayey nannofossil ooze and nannofossil ooze, but generally contain fewer clay-rich intervals than sediments from above. Sedimentation rates are much higher than in the upper intervals (see "Sedimentation Rates" section, this chapter) which suggests that the decreased percentage of clay material results from greater input of carbonate material. Nannofossils dominate the overall sediment composition and several layers contain >90% nannofossils. Basal sediments are marked by increased occurrences of manganese and iron oxide sediments, which often form small pods within the sediment.

BIOSTRATIGRAPHY

A continuous sedimentary record from the upper Pleistocene through the uppermost Miocene was recovered from the five holes cored at Site 853. Calcareous nannofossils provide a well-constrained stratigraphy, which can be calibrated to the paleomagnetic stratigraphy obtained from Site 853. A comparison of the paleomagnetic and nannofossil stratigraphies provides new biochronological data on the calibration of selected nannofossil events in this interval. The following report deals with the biostratigraphic results from Hole 853B, which are illustrated in Figure 11.

Abundance and preservation of the microfossil groups vary throughout the section. Calcareous nannofossils are generally abundant and well to moderately-well preserved. Planktonic foraminifers are poorly preserved and are abundant only in the Pleistocene and Pliocene interval (Cores 138-853B-1H through -4H). In this same interval, radiolarians and diatoms are rare and poorly preserved, while they are present as scattered fragments in the Miocene interval (Core 138-853B-5H through the bottom of the sequence).

In Figure 11, the epoch boundaries have been placed as follows:

Boundary	Hole	Depth (mbsf)	Event
Pleistocene/Pliocene	853B	7.90	Olduvai (t)
Pliocene early/late	853B	16.65	Gauss/Gilbert
Pliocene/Miocene	853B	29.32	T *Discoaster quinqueramus*

T = top occurrence; (t) = termination.

Calcareous Nannofossils

Calcareous nannofossils recovered at Site 853 represent a stratigraphic succession from the upper Pleistocene (Zones CN14b from Okada and Bukry, 1980, and NN20 from Martini, 1971) to the upper part of the upper Miocene (Zones CN8 and NN10). Nannofossils are generally abundant or common throughout the section, and show good to moderately good preservation. In some samples (from Core 138-853B-3H) within the Pliocene interval, assemblages with rare and poorly preserved nannofossils are observed, together with common reworked forms from upper Miocene (Zones CN9, CN7, and CN6). The biostratigraphic events identified in the sedimentary sequence of Site 853 are reported in Table 2.

In the Pleistocene interval (Sections 138-853B-1H-1 through -2H-2) nannofossils are abundant and the assemblage is characterized by *Calcidiscus* spp., helicoliths, ceratolithids, and different morphotypes of *Gephyrocapsa* spp. The nannofossil event that approximates the Pleistocene/Pliocene boundary is the first occurrence of *Gephyrocapsa oceanica* s.l., recorded between Samples 138-853B-2H-2, 140 cm, and -2H-3, 25 cm.

The Pliocene (Sections 138-853B-2H-3 through -4H-CC) is characterized by a rich and diversified nannofossil assemblage, with abundant discoasterids. The last occurrence of *Discoaster brouweri* is recorded between Samples 138-853B-2H-3, 25 cm, and -2H-3, 65 cm. The nannofossil event that approximates the upper/lower Pliocene boundary (Gauss/Gilbert boundary) is the last occurrence of *Reticulofenestra pseudoumbilicus,* recorded between Samples 138-853B-3H-4, 65 cm, and -3H-4, 140 cm. Ceratolithid species *Amaurolithus primus, Amaurolithus delicatus, Amaurolithus tricorniculatus,*

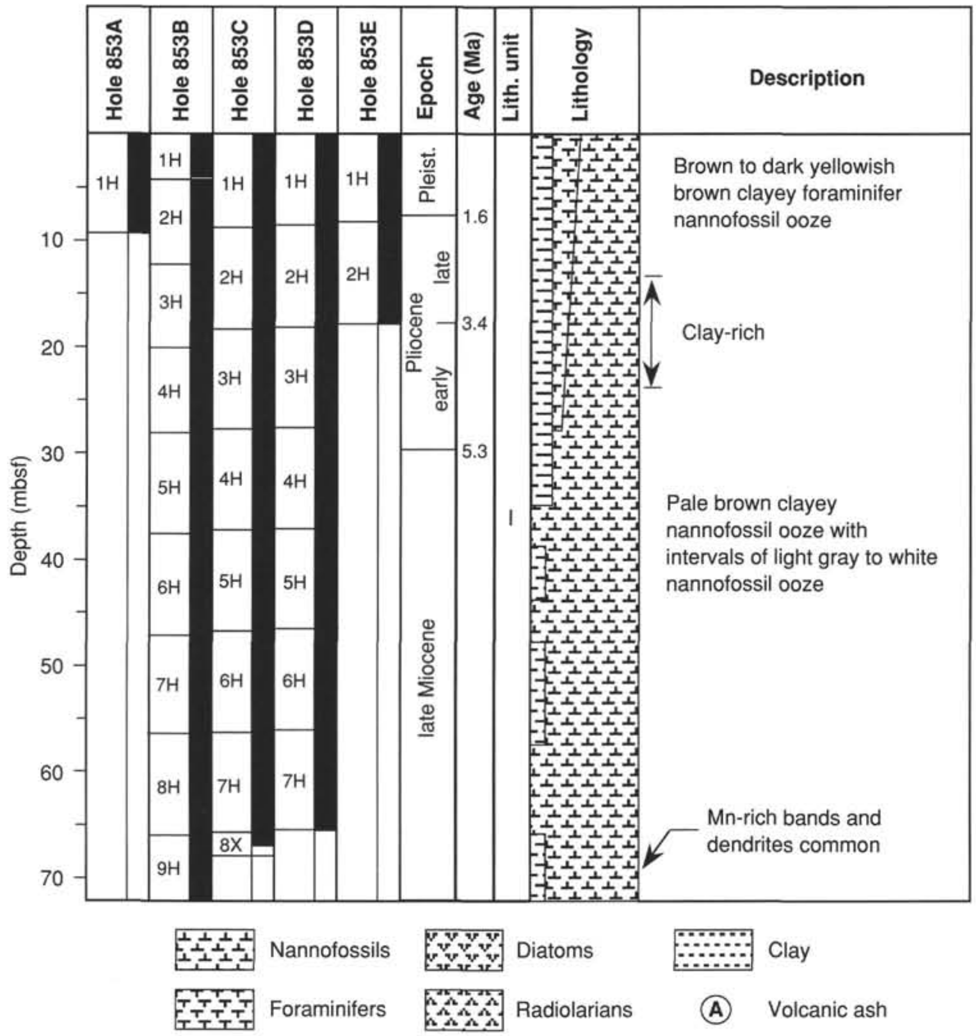

Figure 5. Lithostratigraphic summary of Site 853.

Ceratolithus acutus, Ceratolithus armatus, and *Ceratolithus rugosus* are common to rare in the lower Pliocene interval (Core 138-853B-4H), and intergraded morphotypes between the various species were commonly observed.

The last occurrence of *Discoaster quinqueramus* (top of Zones CN9 and NN11), which approximates the Pliocene/Miocene boundary, was observed between Samples 138-853B-5H-1, 65 cm, and -5H-1, 140 cm. In the interval corresponding to Subzone CN9b (upper part of Zone NN11), *A. primus, A. delicatus,* and *Amaurolithus amplificus* are present, and *Discoaster berggreni* and *D. quinqueramus* dominate the assemblage throughout the Zone CN9 (NN11). Their first occurrence (Zone CN9/CN8 and NN11/NN10 boundary) was recorded between Samples 138-853B-8H-4, 65 cm, and -8H-4, 140 cm.

The lowermost part of the sequence at Site 853 (from Sections 138-853B-8H-5 through -9H-CC) is placed in Zone CN8 (NN10). In this interval the nannofossil assemblage is characterized by abundant and slightly overgrown discoasterids, among which *Discoaster neohamatus* and the *Discoaster bellus* group dominate. Common *Minylitha convallis* and abundant *Sphenolithus abies* were observed. This biostratigraphic assignment indicates an age younger than 8.8 Ma for the lowermost portion of the recovered section.

Planktonic Foraminifers

Planktonic foraminifers are poorly preserved throughout the sedimentary sequence obtained in Hole 853B. In the interval from Cores 138-853B-1H through -4H, planktonic foraminifers are abundant with the exception of Sample 138-853B-3H-CC, in which they are rare. The assemblages exhibit a high degree of fragmentation and consist largely of the robust species *Globorotalia tumida* and numerous keel fragments of this species. The abundance of planktonic foraminifers decreases downward in the remainder of the section. They are common in Sample 138-853B-5H-CC, few in Sample 138-853B-6H-CC, and rare in the interval from Samples 138-853B-7H-CC through -13H-CC. Other coarse fraction components include benthic foraminifers (rare to few in Cores 138-853B-1H through -6H, and common in Cores 138-853B-7H and -9H), and rare to few radiolarians, echinoid spines, and ostracods from Cores 138-853B-2H through -8H. Fish teeth are rare in Cores 138-853B-5H through -7H. Volcanic glass is common in Cores 138-853B-7H through -9H. Manganese micronodules are common to abundant in the lower stratigraphic interval in Cores 138-853B-8H and -9H.

Planktonic foraminiferal datums identified in the sequence are reported in Table 3. The occurrence of sinistrally coiled *Pulleniatina*

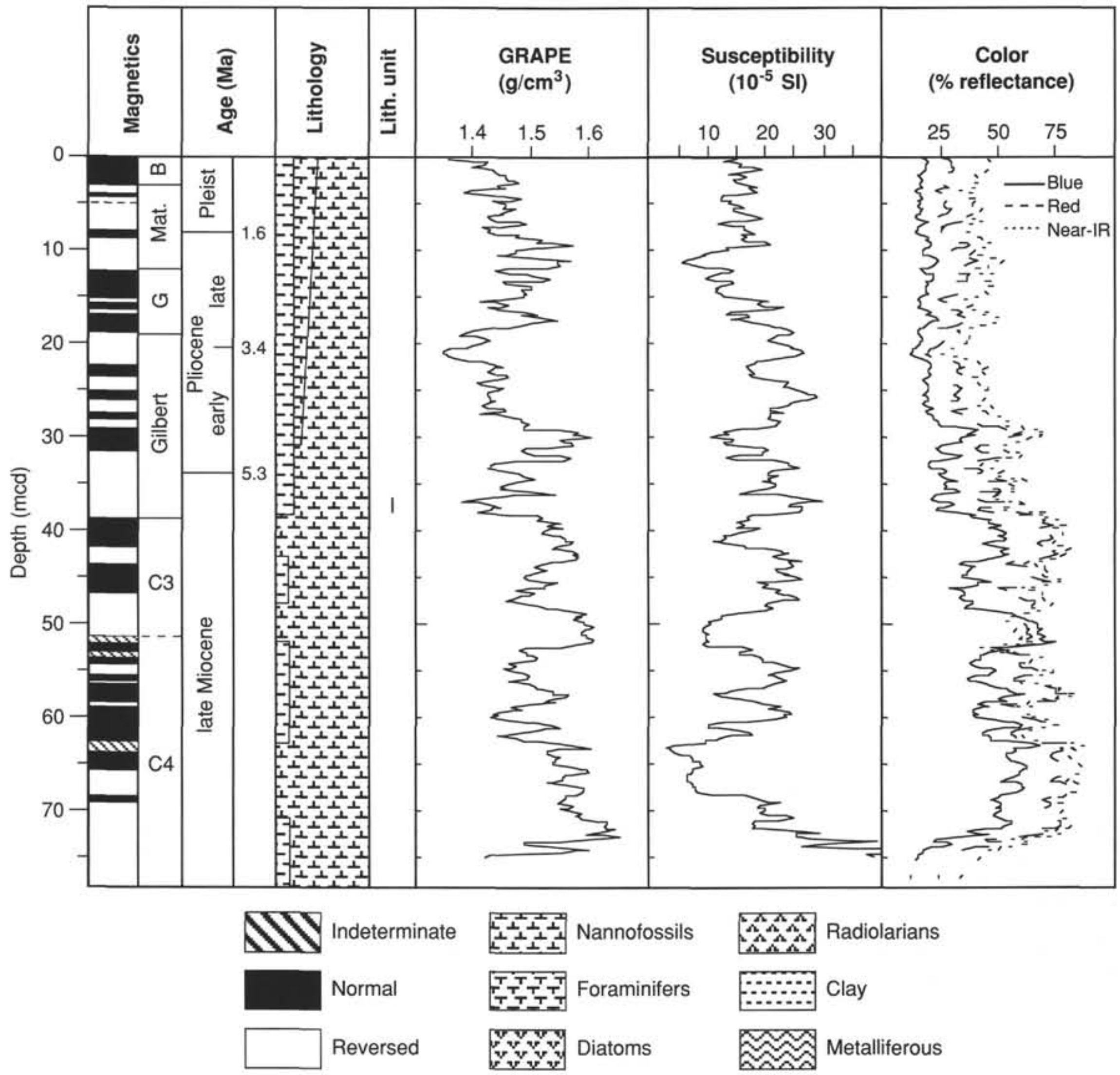

Figure 6. Composite summary of magnetics, age, graphic lithology, GRAPE density, magnetic susceptibility, and color reflectance for Site 853. Composite data consist of sections spliced together from the multiple holes drilled at the site. Data are shown plotted vs. meters composite depth (mcd), the new depth scale used when constructing composite sections. GRAPE, susceptibility, and color data have been smoothed using a 20-point Gaussian filter.

obliquiloculata in Sample 138-853B-1H-CC indicates an age greater than 0.8 Ma for this level. The interval from Cores 138-853B-1H through -2H is assigned to the Pleistocene–upper Pliocene zonal interval N22–N21 based on the simultaneous first occurrences of *Globorotalia limbata* and *Sphaeroidinellopsis* spp. in Sample 138-853B-2H-CC. The base of lower Pliocene Zone N18 is placed in Sample 138-853B-4H-CC at the first occurrence of *Globorotalia tumida.* The remainder of the sequence from Cores 138-853B-5H through -9H is unzoned. This interval yielded nondiagnostic assemblages that consisted mainly of the robust forms *Globoquadrina venezuelana* and *Sphaeroidinellopsis* spp., which are resistant to dissolution.

Radiolarians

Radiolarians sampled in Site 853 are from the Quaternary and upper Pliocene (*Pterocanium prismatium* Zone). Below the top of Core 138-853B-3H, all samples examined are barren of siliceous microfossils. Trace fragments of tests are found in a few of the deeper samples; however, these are never adequate for an evaluation of the age of the sediment or the character of the assemblage. Within the Pliocene–Pleistocene part of the section preservation is poor to moderate, and only a few of the radiolarian datums can be identified with any certainty (Table 4).

Reworking of upper Miocene radiolarians is found in all the Pliocene–Pleistocene samples. This occurrence of reworking is similar to that found at Site 852; however, we were surprised to find comparatively well-preserved Miocene forms in a poorly preserved, younger assemblage, when the upper Miocene section at this site does not appear to contain any siliceous microfossils. This suggests that upper Miocene siliceous microfossils were deposited in this region (but were removed from the thicker sections by post-depositional dissolution) and are being eroded from nearby outcrops of upper Miocene sediments.

Diatoms

With the exception of Samples 138-853A-1H-CC, -853B-1H-CC, and -853B-2H-CC, diatoms are not observed in the core-catcher samples examined from Holes 853A and 853B. Samples 138-853A-

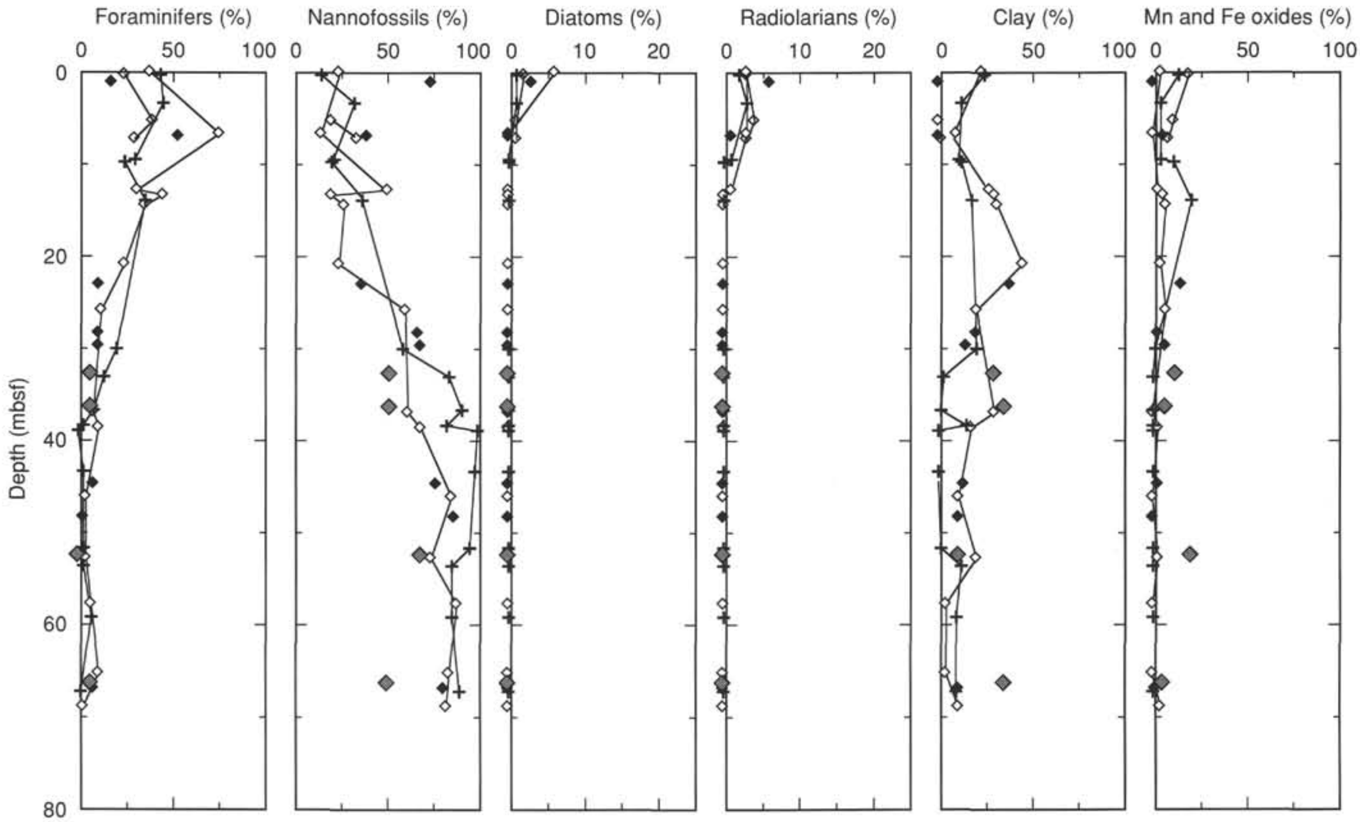

Figure 7. Summary of major (lines) and minor (symbols only) component smear slide data from Site 853.

1H-CC and -853B-1H-CC contain rare and poorly preserved diatoms. Species observed include *Azpeitia nodulifer, Thalassionema nitzschioides,* and fragments of *Ethmodiscus rex.* No age-diagnostic species were observed in these two samples. Sample 138-853B-1H-CC contains few diatoms exhibiting moderate preservation. The occurrence of *Nitzschia fossilis, Nitzschia reinholdii,* and the silicoflagellate *Mesocena quadrangula* allowed us to tentatively place this sample into the Subzone B of the *Nitzschia reinholdii* zone. However, neither *Pseudoeunotia doliolus* nor *Rhizosolenia praebergonii* were observed in this sample.

PALEOMAGNETISM

Procedures

We followed the usual procedures for conducting pass-through magnetometer measurements on archive sections before and after a demagnetization treatment of 15 mT (see "Explanatory Notes" chapter, this volume). All APC cores taken from the five holes drilled at Site 853 were run in this manner. We did not conduct shipboard examinations of discrete samples from any of these cores.

Susceptibility measurements were taken for all cores along with other multisensor track measurements. For the most part, measurements were taken using high sensitivity (0.1 scale) and a sampling interval of 5 cm; however, for Sections 138-853B-3H-6 through -6H-7 and for all of Hole 853D, the sensitivity was set to low sensitivity (1.0 scale), and the measurement interval was reduced to 3 cm.

Results

Paleomagnetic Remanence

The remanence intensity of Site 853 sediments is generally in the range of 1–5 mA/m, with slightly higher values in the uppermost several meters (Fig. 12). Although the intensity varies considerably within these sediments, there is no obvious tendency for intensity to decrease downhole, beyond the slight decrease seen within the upper 10 m.

The remanence directions obtained from pass-through measurements indicate that generally an ancient magnetization direction is revealed after the upward vertical overprint is removed with demagnetization (Figs. 13, 14, and 15). However, the 15-mT demagnetization treatment does not result in symmetrical positive and negative inclinations, and we surmise that a residual overprint remains. Nevertheless, the paleomagnetic record from this site contains many sharp 180° shifts in declination, which are often accompanied by reversals in the sign of the inclination. These reversals correlate well between holes (Fig. 16), with the exception of the zone below 62 mcd, for which only Core 138-853D-7H gave interpretable results.

Interpretation

We determined polarity sense in all cores that showed a clear reversal pattern by considering both inclination changes and multishot orientations (Table 5). Despite the low site latitude, the polarity sense can be readily determined because of the considerable overlap available from the multiple holes. In the 10 cores for which the multishot orientations could be compared with a clear reversal pattern (Cores 138-853B-5H, -6H, -7H, -853C-4H, -5H, -6H, -853D-4H, -5H, -6H, -7H), all are consistent with both inclination and with the overall magnetostratigraphic interpretation for this site.

The correlation of the magnetic polarity zonation obtained with the magnetic polarity timescale (MPTS; see Fig. 16; Table 6) is consistent with the shipboard nannofossil biostratigraphy. Key constraints include the identification of LO *D. quinqueramus* (4.98 Ma) at the top of Core 138-853B-5H, FO *A. primus* (6.70 Ma) in the upper

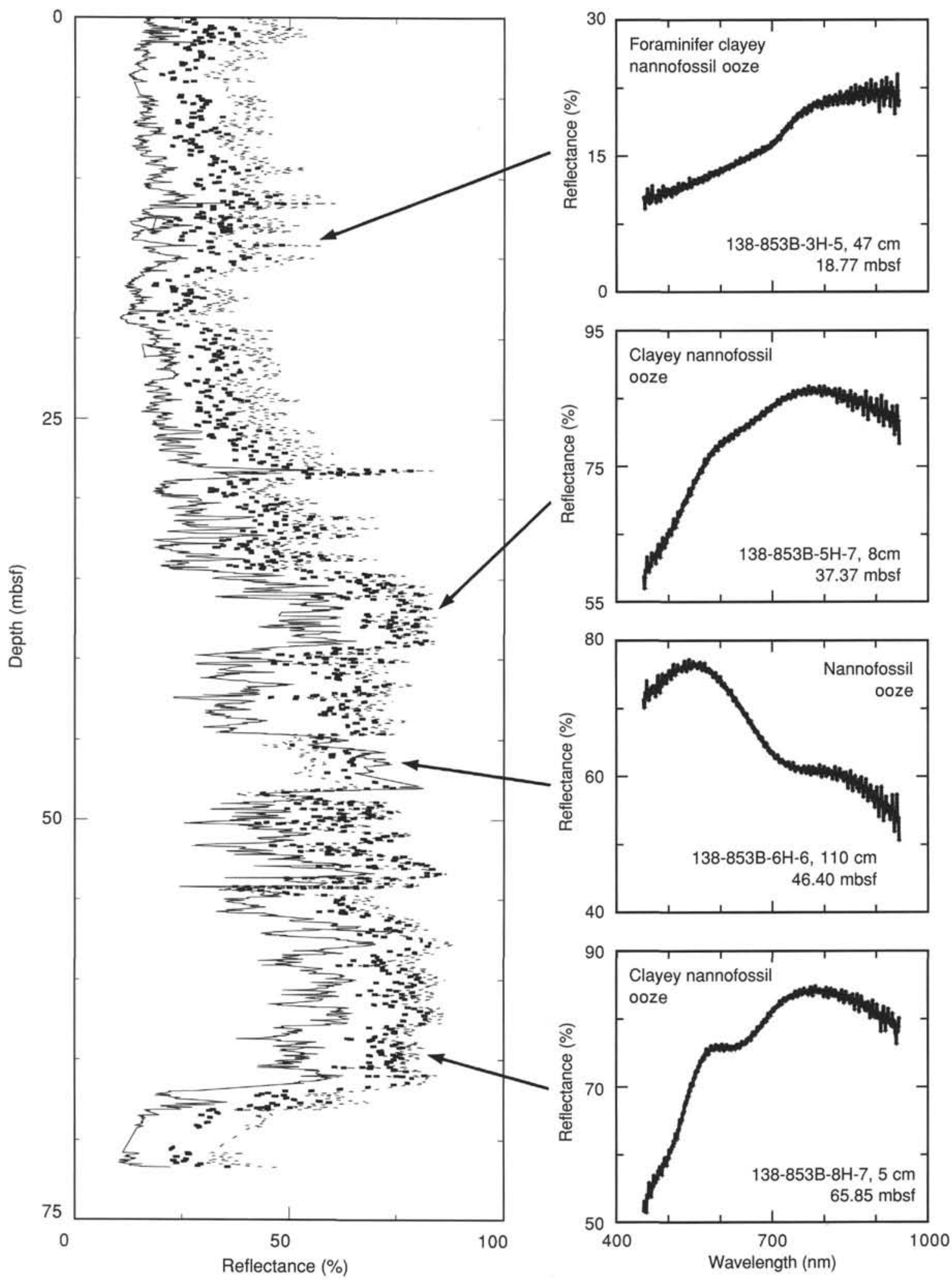

Figure 8. Color reflectance data for Hole 853B and wavelength spectrum for specific lithologies within the core, blue = solid line; red = coarse dashed line; near-infrared = fine dashed line.

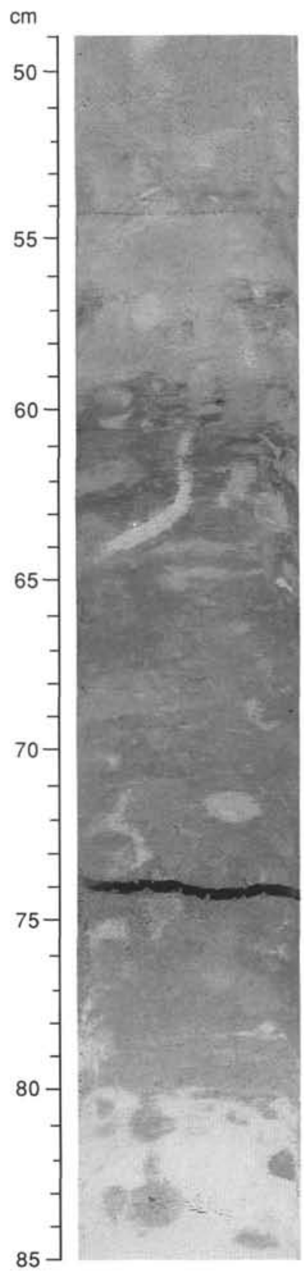

Figure 9. Bioturbation within a darker oxide-rich bed in Section 138-853C-4H-5 at 49–85 cm.

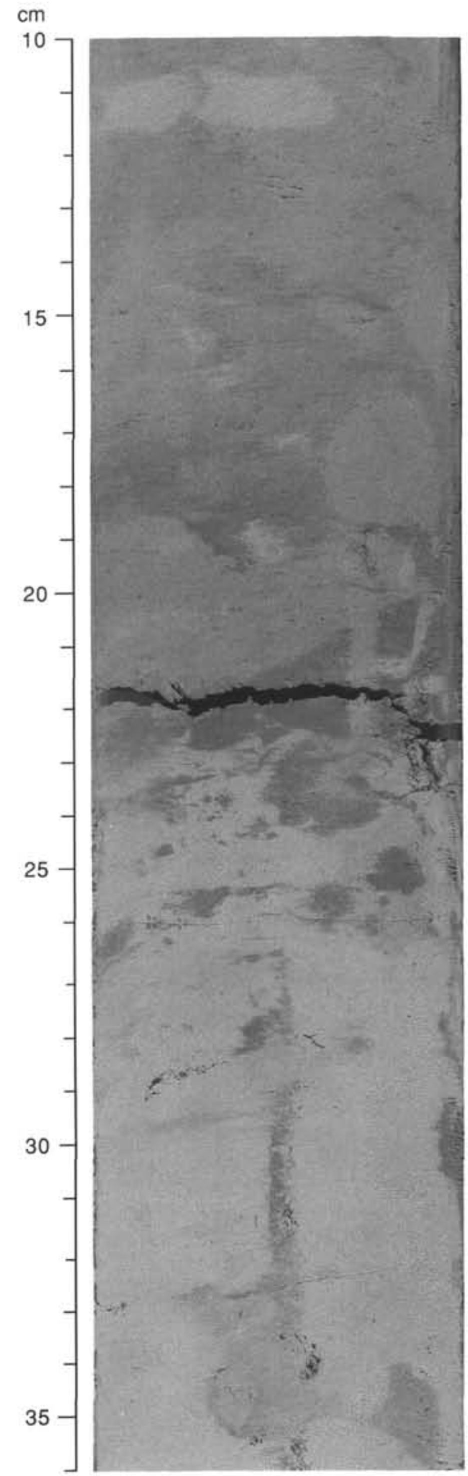

Figure 10. A vertical *Skolithos* burrow cut by solid burrows below a darker oxide-rich bed in Section 138-853C-4H-5 at 10–36 cm.

part of Core 138-853B-7H and FO *D. berggreni* (7.5 Ma) in Section 4 of Core 138-853D-8H (see "Biostratigraphy" section, this chapter). For the most part, the assignment of polarity zones was straightforward; however, a number of minor difficulties arose that might have stemmed from the presence of short polarity zones not recognized in standard time scales. For example, the short reverse polarity zone at 56 mcd may correspond to the lowermost C3A-r3, if the short normal above it is taken as reflecting a newly recognized subchron (as we have done, e.g., in Sites 844 and 845). Alternatively, this narrow reverse interval might itself constitute a short reverse zone within C4-n1 that is not reflected in the magnetic polarity timescale. A better understanding of what appear to be various short polarity intervals and a more firm correlation of these to the MPTS will certainly require further shore-based effort.

Low-Field Susceptibility

Like remanence, the susceptibility signal varies considerably over narrow intervals, but does not show an overall downhole decrease. The average value of susceptibility remains ~10^{-4} SI and does not show any decrease in the upper 10 m where remanence declines. The

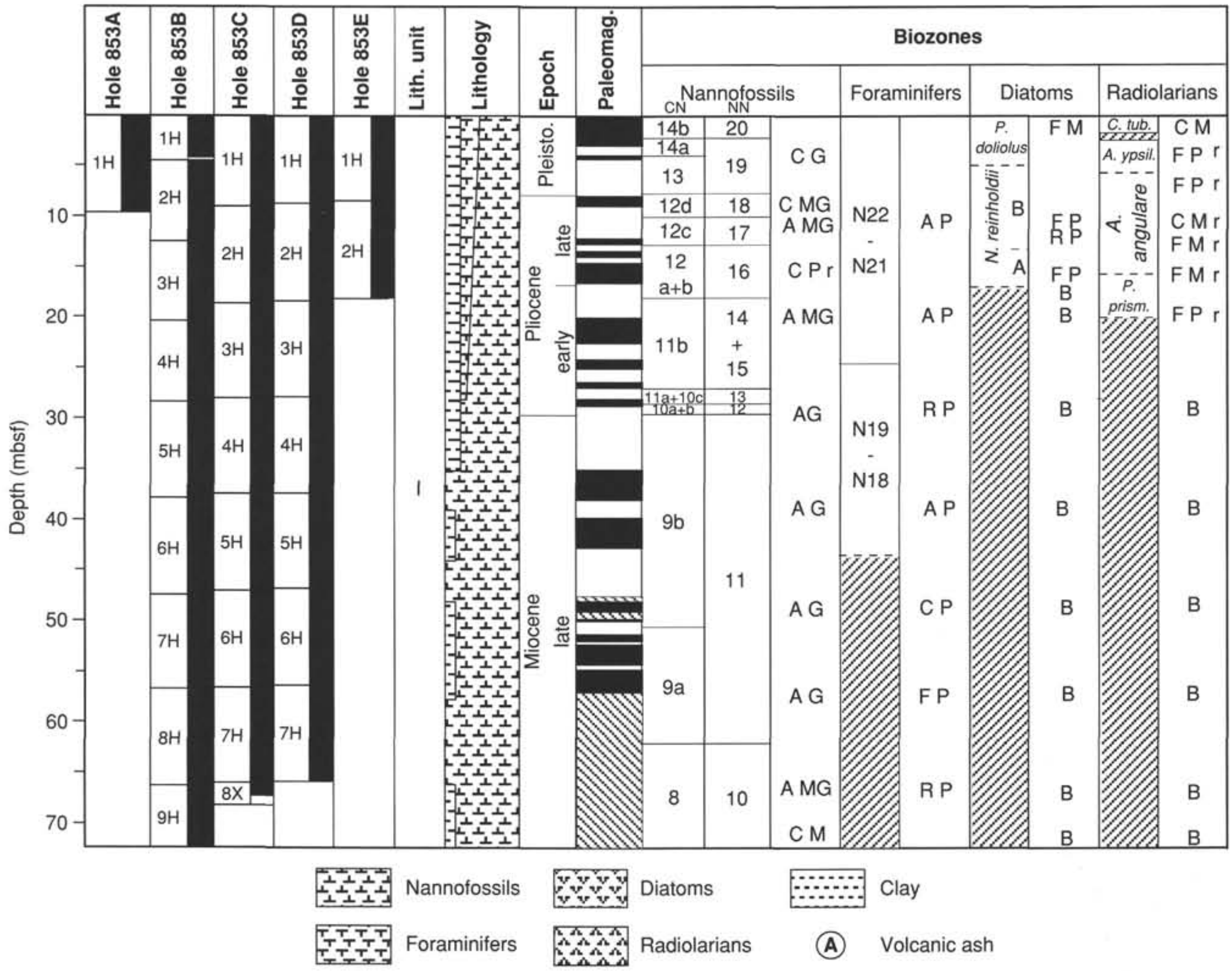

Figure 11. Stratigraphic summary for Site 853. Depth is in meters below seafloor (mbsf). Microfossil abundance recorded as A = Abundant; C = Common; F = Few; R = rare; B = barren. Microfossil preservation recorded as G = good; M = moderate; P = poor. "r" = presence of older reworked microfossils. This figure is a general overview of the stratigraphic results at Site 853. Placement of specific stratigraphic boundaries may differ slightly between Holes 853B, 853C, and 853D.

susceptibility variations correlate reasonably well with similar variations in remanence intensity (Fig. 12) and also show a clear correspondence with changes in sediment color (Fig. 17); yellow-brown intervals correspond to higher susceptibility and remanence while blue-gray zones have lower susceptibility and remanence. Presumably both sediment color and these magnetic parameters are simply reflecting the differences between more oxidized and more reduced zones within the section, where iron oxide minerals are more or less well preserved. Other factors, such as the dilution of terrigenous input by carbonate, presumably also play significant roles in controlling the magnetic susceptibility and remanence signals.

SEDIMENTATION RATES

A sedimentary section ~70 m thick covering the time interval from the late Pleistocene to the base of the late Miocene was recovered at Site 853. Biostratigraphic age control was somewhat reduced at Site 853 but sufficient constraint was provided by the four chief planktonic microfossil groups to ensure that the excellent magnetostratigraphic record was properly interpreted.

The composite depth section for Site 853 is given in Table 7. This composite was formed by comparing shipboard measurements of GRAPE density, magnetic susceptibility, and percent reflectance (from the automated color analyzer) at adjacent holes. These comparisons were then integrated to form a single composite depth section for the site (a detailed discussion on the construction of composite sections during Leg 138 is presented in Hagelberg et al., this volume).

For the holes and cores listed in Column 1 of Table 8, Column 2 gives the ODP sub-bottom depth of each core's top and bottom (in meters below seafloor, or mbsf). Note that the depth given in Column 2 corresponds to the depth of the bottom of the recovered core. This depth places the core catchers in their correcct position in the composite depth section and is not the same as the standard ODP core-catcher depth. Column 3 shows the length of core recovered. Column 4 gives the composite depth of each core's top and bottom (in meters composite depth, or mcd). Column 5 indicates the amount of offset between the ODP depth and the composite depth. ODP sub-bottom depths can be converted to composite depths by adding the offset listed in Column 5 for a given core.

GRAPE density, susceptibility, and percentage of reflectance data all produced records with relatively high amplitudes and variability throughout much of the section in Holes 853A (1 core), 853B (9 cores), 853C (8 cores), 853D (7 cores), and 853E (2 cores) at Site 853 (Fig. 18, back pocket). Weather conditions resulted in large ship's

Table 2. Sample and depth constraints of calcareous nannofossil events for Site 853.

Event	Hole 853B		
	Interval	Depth (mbsf)	Depth (mcd)
T *Pseudoemiliania lacunosa*	1H-2, 65–1H, 130	2.15-2.80	2.15-2.80
B *Gephyrocapsa* sp.3	1H-3, 40–1H-CC	3.40-4.25	3.40-4.25
T *Calcidiscus Macintyrei*	2H-2, 65–2H-2, 140	6.45-7.20	6.45-7.15
B *Gephyrocapsa oceanica* s.l.	2H-2, 140–2H-3, 25	7.20-7.55	7.15-7.50
T *Dicoaster brouweri*	2H-3, 25–2H3, 65	7.55-7.95	7.50-7.90
T *Dicoaster pentaradiatus*	2H-5, 65–2H-5, 140	10.95-11.70	10.90-11.65
T *Discoaster surculus*	2H-6, 65–2H-6, 140	12.45-13.20	12.40-13.15
T *Sphenolithus* spp.	3H-4, 65–3H-4, 140	17.45-18.20	19.85-20.60
T *Reticulofanestra pseudoumbilicus*	3H-4, 65–3H-4, 130	17.45-18.20	19.85-20.60
B *Discoaster asymmetricus*	4H-5, 65–4H-5, 140	26.95-27.70	27.95-28.70
T *Ceratolithus acutus*	4H-5, 140–4H-6, 80	27.70-28.60	28.70-29.60
B *Ceratolithus rugosus*	4H-6, 80–4H-CC	28.60-28.89	29.60-29.89
B *Ceratolithus acutus*	5H-1, 65–5H, 140	28.95-29.70	32.40-33.15
T *Discoaster quinqueramus*	5H-1, 65–5H-1, 140	28.95-29.70	32.40-33.13
T *Amaurolithus amplificus*	5H-5, 65–5H-5, 140	34.95-35.70	38.40-39.15
B *Amaurolithus amplificus*	6H-4, 27–6H-4, 65	42.57-42.95	46.37-46.75
B *Amaurolithus primus*	7H-2, 147–7H-3, 30	50.27-50.60	54.42-54.75
B *Discoaster berggreni*	8H-4, 65–8H-4, 140	61.95-62.70	67.20-67.95

T = top; B = bottom.

Table 3. Sample and depth constraints of foraminifer events for Site 853.

Event	Hole 853B		
	Interval	Depth (mbsf)	Depth (mcd)
Occurence left-coiling *Pulleniantina obliquiloculata*	1H-CC	4.25	4.25
T *Globorotalia limbata*	1H-CC–2H-CC	4.25–14.11	4.25–14.06
T *Sphaeroidinellopsis spp*	1H-CC–2H-CC	4.25–14.11	4.25–14.06
B *Globorotalia tumida*	4H-CC–5H-CC	29.89–38.17	29.89–41.62

Table 4. Sample and depth constraints of radiolarian events for Site 853.

Event	Hole 853B		
	Interval	Depth (mbsf)	Depth (mcd)
T *Stylatractus universus*	1H-1–1H-2	1.1–2.6	1.1–2.6
T *Anthocyrtidium angulare*	1H, CC–2H-1	4.25–5.4	4.25–5.35
T *Theocorythium vetulum*	1H, CC–2H-1	4.25–5.4	4.25–5.35
B *Theocorythium trachelium*	2H-3–2H-4	5.45–8.40	5.45–8.35
T *Pterocanium prismatium*	2H-1–2H-3	8.4–9.9	8.35–9.85
T *Lamprocyrtis heteroporos*	2H-1–2H-3	5.4–8.4	5.35–8.35

T = top; B = bottom.

heave from swells at this site. Consequently, we found it difficult to maintain offset depths in adjacent holes during drilling; thus, the GRAPE record showed some distortions reflecting damage to the core liner, e.g., in Hole 853D alone, successive cores showed a range from a 2.3-m gap to a 1-m overlap. Despite these difficulties, overlap of adjacent holes was maintained throughout the cored section at Site 853 except for one interval, between Cores 138-853C-5H and -853B-7H (at ~52 mcd) where the overlap shown in Figure 18 (back-pocket) is not well substantiated.

To learn more about the nature of the mechanism by which the APC-coring process produces gaps between successive cores, part of Hole 853B (Cores 138-853B-3H through -5H) was recovered with a nominal 8 m advance between cores instead of the standard 9.5 m advance. This experiment was less useful than hoped because the sea conditions were worse at this site than at any other site drilled during Leg 138. The offsets for these three cores seem more variable than the offsets of other cores at Site 853 (see Table 7), but we do not know whether this was because of sea conditions or whether it was more difficult to accurately judge 8-m advances. However, our chief objective was to establish whether the material that is apparently unrecovered between successive standard 9.5 m advances has survived undisturbed, such that it might be recovered by making shorter advances between APC deployments. This objective was not achieved because Cores 138-853B-3H and -853B-5H took sediment starting below the bottom of their preceding cores, despite the nominal 8-m advance, while Core 138-853B-4H actually duplicated the bottom 1 m of Core 138-853B-3H with both pristine GRAPE and susceptibility records (Fig. 18, back pocket) and an undisturbed paleomagnetic record. Thus, the drill pipe must have moved laterally, and we cannot judge whether the material immediately below the bottom of Core 138-853B-3H could have been recovered intact or not.

The sedimentation rate record for Site 853 was based almost entirely on the very clear paleomagnetic record from the Brunhes down to C4-n2 (older than 6.85 Ma). Below this depth, the first appearance of *Discoaster berggreni* (7.5 Ma) between Samples 138-853B-8H-4, 65 cm, and -8H-4, 140 cm (67.57 mcd) was used to constrain the sedimentation rate in the lowest part of the section. Using this datum and extrapolating the same sedimentation rate to the base of the section would imply an age of ~8.7 Ma. This age would be an upper limit based on the absence of *Discoaster hamatus* at the bottom of the section; however, the paleomagnetic record only includes one very short normally magnetized interval (between 68.4 mcd and 69.0 mcd) whereas an age of 8.7 Ma would require that the section penetrated both C4A-n1 and C4A-n2. Further detailed comparisons with other sites will be necessary to evaluate the true age of the base of the section and the pattern of sedimentation rate change in the lowest 10 m. Table 8 gives the control points selected to generate the plot of age vs. depth in Figure 19, where the depth ranges within which the datums for the nannofossils that were observed are shown.

The pattern of sedimentation rate variation vs. age (Fig. 20) and depth (Fig. 21) has some resemblance to that of Sites 848–852 despite the fact that overall rates are so low. Over the past 4 m.y. (0–23 mcd) the rates are low, ranging from 4 m/m.y. in the Brunhes to 8 m/m.y. between 2 and 3 Ma. Between 4 and 7.5 Ma the average sedimentation rate was ~14 m/m.y.

INORGANIC GEOCHEMISTRY

Nine interstitial water samples were collected at Site 853, two from Hole 853A at 1.5 and 7.5 mbsf and seven from Hole 853B, from 11.8 mbsf to 65.8 mbsf, just above basement (Table 9). Pore-water results from these two holes are considered to constitute a single depth profile in this report.

An interstitial-water sample was taken from Sections 1 and 5 of the solitary core from Hole 853A. Core 138-853A-1H consists of clayey nannofossil foraminifer ooze with oxides. This sediment contains up to 15% iron oxides (see "Lithostratigraphy" section, this chapter).

Beginning with the second core from Hole 853B, one interstitial water sample was taken from every core in the hole to basement. The dominant lithology in Core 138-853B-2H is clayey nannofossil fora-

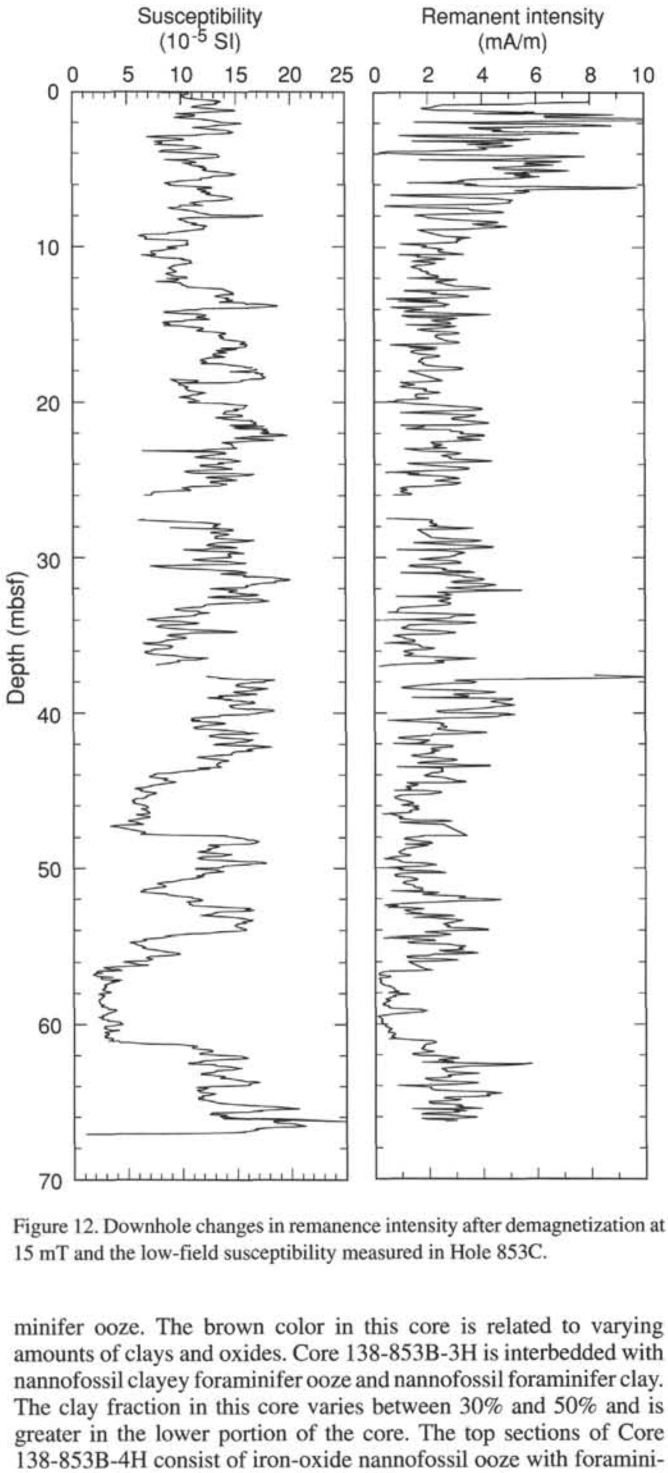

Figure 12. Downhole changes in remanence intensity after demagnetization at 15 mT and the low-field susceptibility measured in Hole 853C.

minifer ooze. The brown color in this core is related to varying amounts of clays and oxides. Core 138-853B-3H is interbedded with nannofossil clayey foraminifer ooze and nannofossil foraminifer clay. The clay fraction in this core varies between 30% and 50% and is greater in the lower portion of the core. The top sections of Core 138-853B-4H consist of iron-oxide nannofossil ooze with foraminifers while Section 138-853B-4H-6 and the core catcher are composed of clayey nannofossil ooze with foraminifers. This latter sediment type dominates the lithology through Core 138-853B-7H.

The first real evidence of hydrothermal influence begins in Core 138-853B-8H with the appearance of manganese dendrites below Section 138-853B-8H-4. The next and last core in this hole (Core 138-853B-9H) is dominated by nannofossil ooze with clay. Several basalt fragments coated with manganese oxide were recovered in Sections 2, 3, and the core catcher.

In general, sediment in Hole 853B consists of nannofossil foraminifer ooze with clays and varying amounts of oxide. The prominence of clays and oxides at Site 853 is consistent with the lower sedimentation rates (see "Sedimentation Rates" section, this chapter).

As at Site 852, the smell of H_2S is completely absent at Site 853 and ammonia levels are <10 µM (Table 9). These observations, together with the low sedimentation rates (see "Sedimentation Rates" section, this chapter) and low organic carbon content (see "Organic Geochemistry" section, this chapter), would suggest that the sediments at Site 853 might be oxidizing throughout. This prediction is borne out by the chemistry of the pore water (Table 9).

The total spread in interstitial sodium (Fig. 22A) and chloride (Fig. 22B) concentrations at this site are 0.5% and 0.8%, respectively. These variations are within the uncertainties of these measurements.

The greatest alkalinity at Site 853 occurs in the uppermost sample (Fig. 22C), with a decreasing trend downhole. This profile suggests that early diagenesis is confined to the sediment/water interface where oxygen and nitrate are consumed to oxidize organic matter (Froelich et al., 1979). Early diagenesis produces pore water with alkalinity slightly higher than bottom water without consuming sulfate, as observed at Site 853.

The highest alkalinity achieved at this site (2.796 mM) is similar to, but less than the highest alkalinity achieved at Site 852 (3.052 mM). Unlike the previous site, alkalinity does not remain at this level in the upper sediment layers but decreases linearly downhole. These differences reflect the thinner sediment cover at this site combined with an even lower organic carbon burial rate (see "Organic Geochemistry" section, this chapter). Slower burial causes alkalinity to be produced closer to the interface, allowing for more effective diffusive communication with bottom water. The linear trend to basement implies diffusional control with a crustal end-member possessing a bottom water alkalinity.

Sulfate at Site 853 (Fig. 22D) is almost constant with depth. The total range in sulfate is 2.5% relative, within the realm of analytical uncertainty. Since sulfate is not being reduced at this site, one would not expect to see the decreasing magnesium and calcium concentrations associated with calcium carbonate precipitation (Baker, 1986; Suess, von Huene, et al., 1988; Pedersen and Shimmield, 1991). Magnesium (Fig. 23A) and calcium (Fig. 23B) are consistent with this picture. The total change in magnesium and calcium is 1.8% and 3.8%, respectively, with no discernable trend with depth.

Interstitial silica at this site has an unusual profile with depth (Fig. 23D). This profile is not easily explained, as it does not seem to be predicted by reactions for the known sources or sinks for silica in deep-sea sediments. The observation that these silica levels are lower than at other Leg 138 sites probably reflects the low abundance of siliceous microfossils in Site 853 sediments (see "Biostratigraphy" section, this chapter.

This site is the first location on Leg 138 where interstitial strontium does not show a clear maximum at depth (Fig. 24B). This result is consistent with the previous conclusion (see "Inorganic Geochemistry" section, "Site 851" chapter, this volume) that the amount of strontium released during recrystallization is directly related to the corrosiveness of the pore water, and thus to the extent of diagenesis. It is clear that the burial rate of organic carbon at this site is so low that early diagenesis occurs very near or at the sediment/water interface, allowing most of the corrosive character produced by oxidation of organic matter to escape to bottom water before burial. The most direct indication of this "equilibration" process is pH; the range in pH at Site 852 is 7.09–7.22 while it is 7.52–7.62 at this site (Table 9).

Lithium (Fig. 24A) is consistent with the strontium profile. Site 853 is the first site on Leg 138 where lithium does not decrease with depth. In fact, lithium concentrations are somewhat higher than bottom water below the top sections.

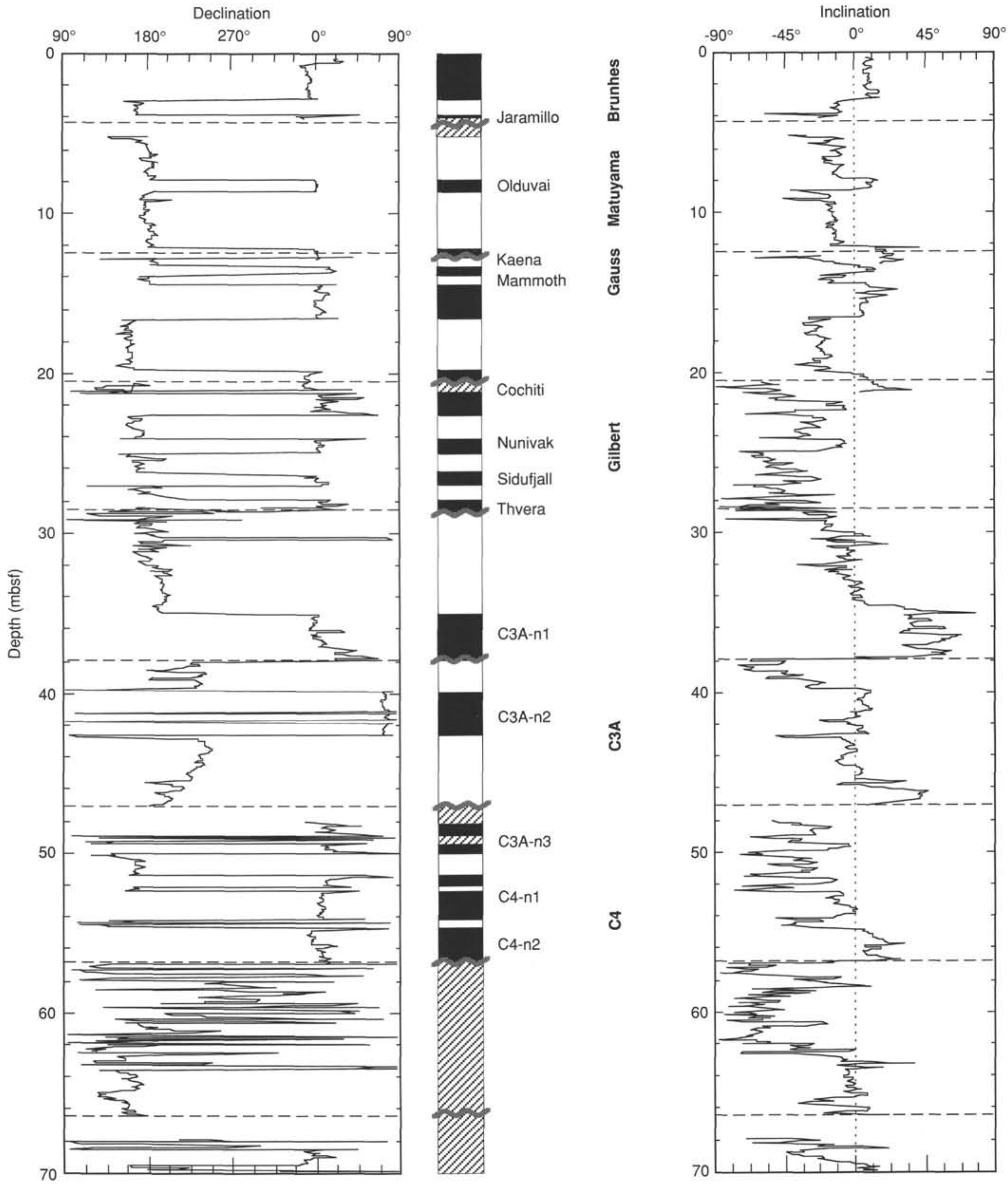

Figure 13. Declination and inclination profiles from the pass-through magnetometer (demagnetized at 15 mT) and identification of polarity chronozones in Hole 853B (black = normal, white = reverse, hatched = no data or no interpretation; dashed lines = core boundaries). Declinations have been rotated as described in Table 5.

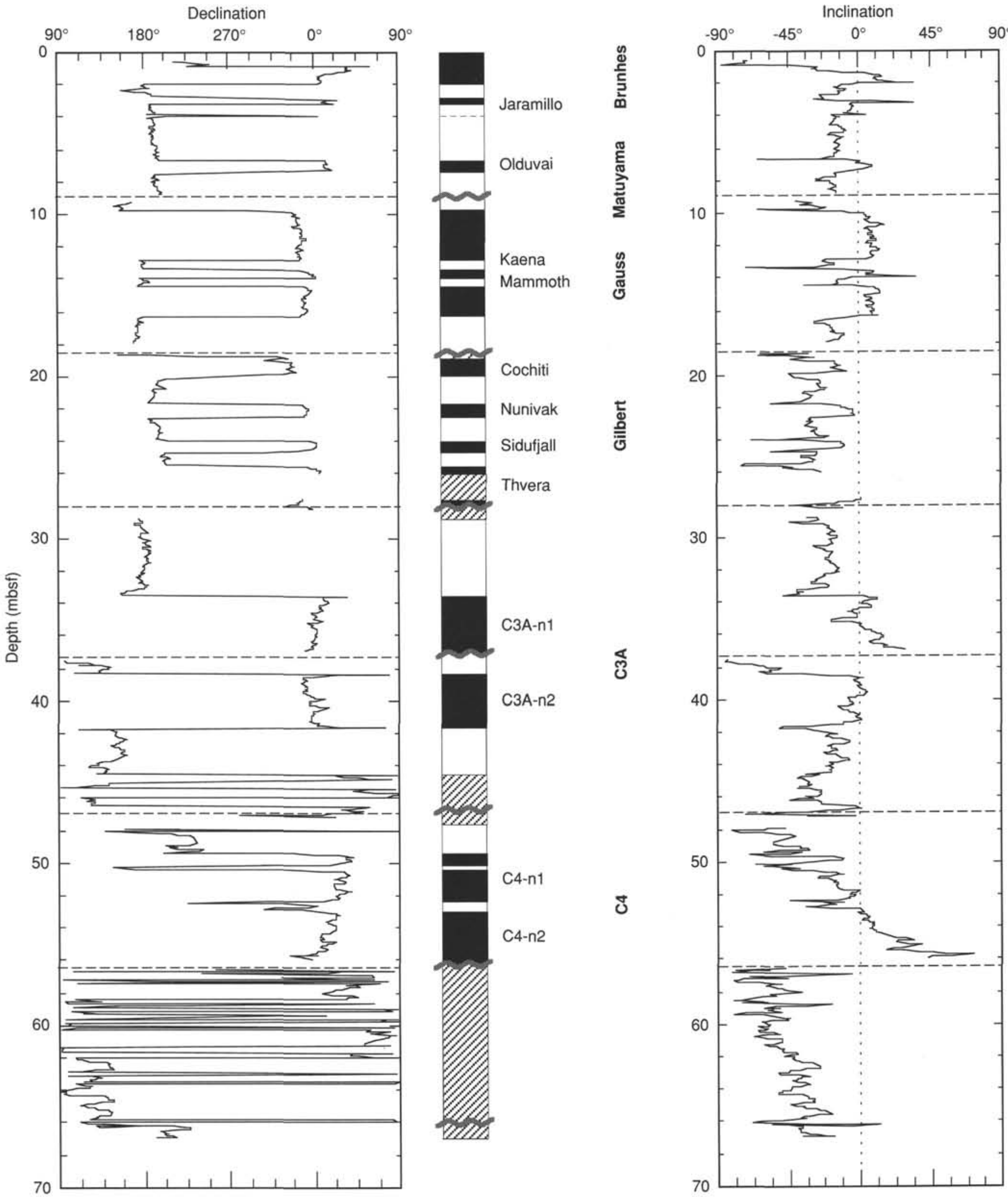

Figure 14. Declination and inclination profiles from the pass-through magnetometer (demagnetized at 15 mT) and identification of polarity chronozones in Hole 853C (black = normal, white = reverse, hatched = no data or no interpretation; dashed lines = core boundaries). Declinations have been rotated as described in Table 5.

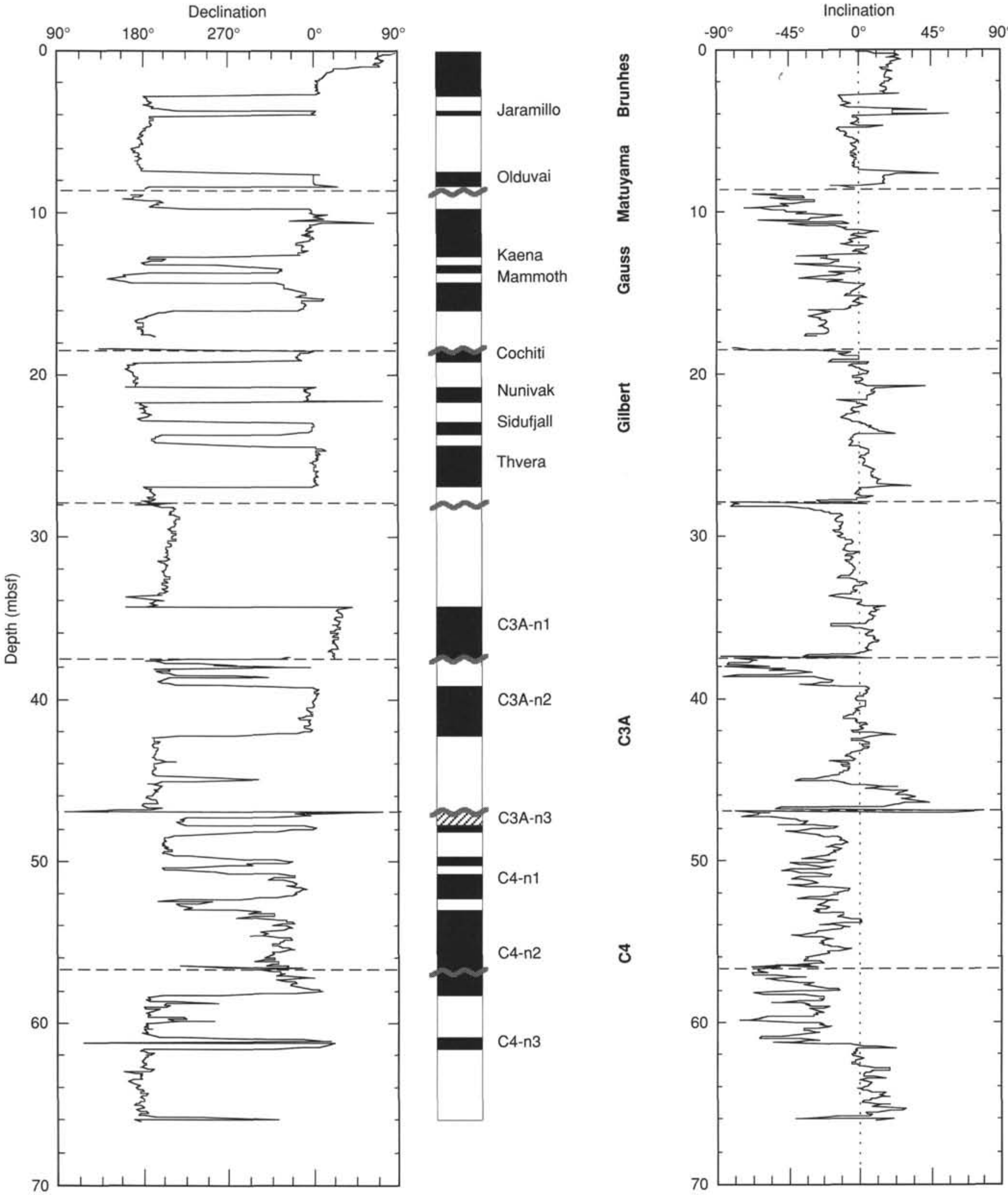

Figure 15. Declination and inclination profiles from the pass-through magnetometer (demagnetized at 15 mT) and identification of polarity chronozones in Hole 853D (black = normal, white = reverse, hatched = no data or no interpretation; dashed lines = core boundaries). Declinations have been rotated as described in Table 5.

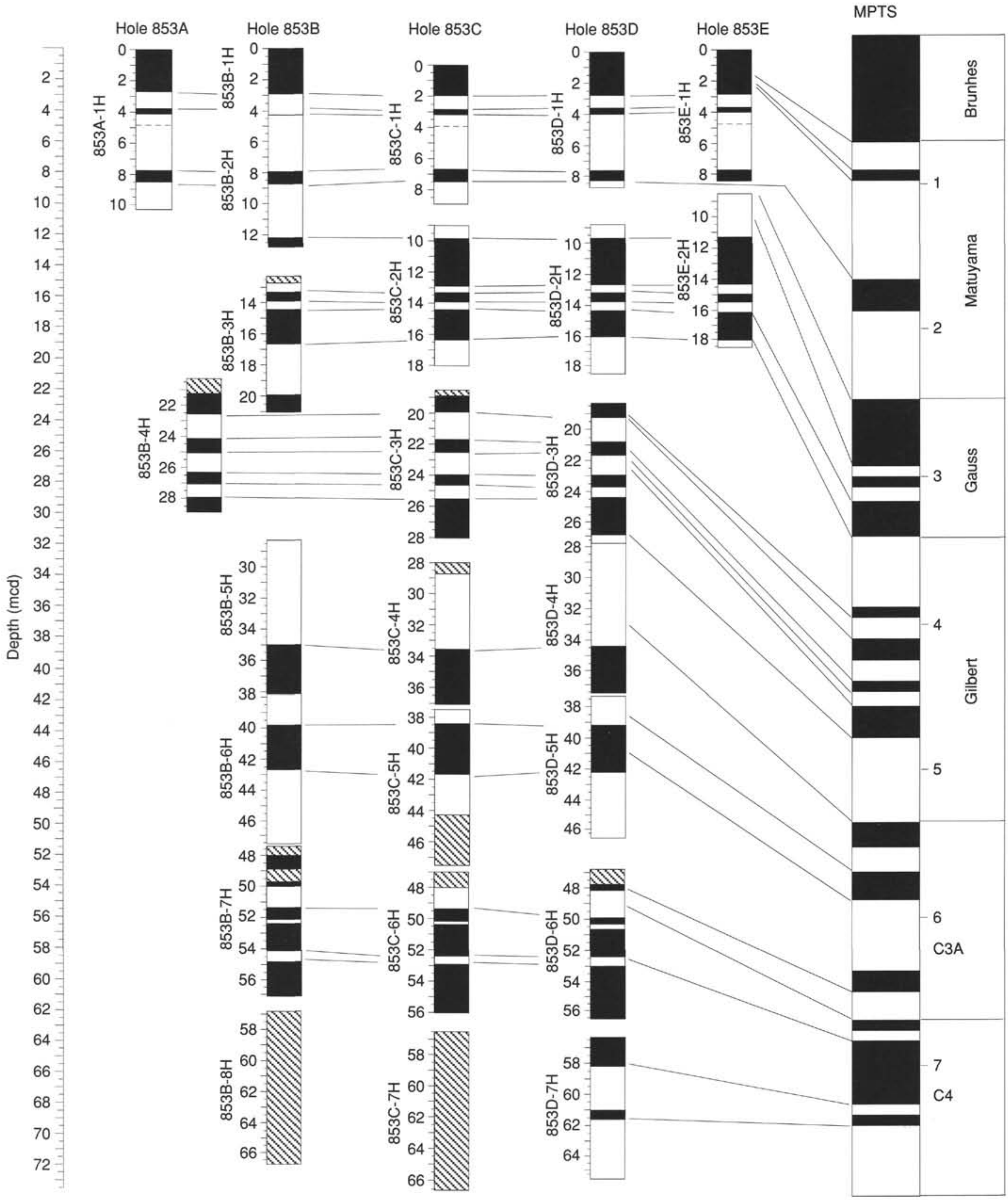

Figure 16. Magnetostratigraphic synthesis at Site 853. Depth ticks on individual cores are in meters below sea floor (mbsf). Cores are located at appropriate composite depth (mcd). Black zones = normal polarity; white zones = reverse polarity; hatched zones not interpreted. MPTS = magnetic polarity timescale.

Table 5. Core orientations for Site 853.

Core no.	Azimuthal orientation (0°–360°)	Deviation from direction (0°–360°)	Vertical drift (°)
138-853A-1H	[a]300		
[a]138-853B-1H	320		
[a]138-853B-2H	210		
[a]138-853B-3H	265		
[a]138-853B-4H	220		
138-853B-5H	183	325	2.7
138-853B-6H	325	336	2.8
138-853B-7H	210	328	2.6
138-853B-8H	270	335	2.8
138-853B-9H	235	330	2.5
[a]138-853C-1H	340		
[a]138-853C-2H	010		
[a]138-853C-3H			
138-853C-4H	273	347	0.8
138-853C-5H	206	100	0.2
138-853C-6H	225	260	0.1
138-853C-7H	237	190	0.3
[a]138-853D-1H			
[a]138-853D-2H			
[a]138-53D-3H			
138-853D-4H	180	140	4.7
138-853D-5H	162	140	4.9
138-853D-6H	058	143	5.5
138-853D-7H	034	140	5.4
138-853E-1H	[a]220		
138-853E-2H	[a]270		
138-853A-1H	[a]300		
[a]138-853B-1H	320		
[a]138-853B-2H	210		
[a]138-853B-3H	265		
[a]138-853B-4H	220		
138-853B-5H	183	325	2.7
138-853B-6H	325	336	2.8
138-853B-7H	210	328	2.6
138-853B-8H	270	335	2.8
138-853B-9H	235	330	2.5
[a]138-853C-1H	340		
[a]138-853C-2H	010		
[a]138-853C-3H			
138-853C-4H	273	347	0.8
138-853C-5H	206	100	0.2
138-853C-6H	225	260	0.1
138-853C-7H	237	190	0.3
[a]138-853D-1H			
[a]138-853D-2H			
[a]138-853D-3H			
138-853D-4H	180	140	4.7
138-853D-5H	162	140	4.9
138-853D-6H	058	143	5.5
138-853D-7H	034	140	5.4
138-853E-1H	[a]270		
138-853E-2H	[a]170		

[a]Secondary orientation (SOR) angle is the value used to adjust average measured declination to 0° or 180° for normal or reversed chronozones, respectively, when no multishot orientation was available. For multishot orientation, the measured declination was corrected by adding it to the multishot azimuthal orientation and the local geomagnetic deviation (8.9°).

In summary, alkalinity and sulfate profiles suggest that early diagenesis at Site 853 is confined to degradation reactions by oxygen and nitrate at or very near the sediment/water interface. In addition, crystallization is nonoperative at this site, leading to limited variations in magnesium, calcium, lithium, and strontium.

ORGANIC GEOCHEMISTRY

Carbonate and Organic Carbon

Inorganic and organic carbon were measured in Hole 853B following the methods outlined in the "Explanatory Notes" chapter (this volume). From the inorganic carbon data, we calculated the weight percent of calcium carbonate (%$CaCO_3$). Percentages of organic carbon (%C_{org}) were determined by measuring the amount of carbon in the dried residues from Coulometer analyses after treatment with 2N HCl (see "Explanatory Notes" chapter, this volume). The analytical results are listed in Table 10 (CD ROM, back pocket) with respect to both ODP depth (mbsf) and to composite depth (mcd; see "Sedimentation Rates" section, this chapter). If a duplicate analysis was performed on a given sample, the mean value of the original analysis and the duplicate is listed in Table 10 (CD ROM, back pocket). Duplicate percentage of $CaCO_3$ analyses are listed in Table 11. The results indicate a reproducibility of 0.9%.

Figures 25 and 26 show percentages of $CaCO_3$ and C_{org} at Site 853 vs. ODP depth and vs. composite depth and age, respectively, based on datum levels identified at Site 853 (see "Sedimentation Rates" and "Paleomagnetism" sections, this chapter). The percent $CaCO_3$ record at Site 853 shows consistently high values (between 60% and 80%) throughout the section. Organic carbon concentrations are low (0.0%–0.1%) throughout.

Accumulation Rates

We calculated the average values of several sedimentary parameters in time intervals delimited by the chronostratigraphic levels discussed in the "Sedimentation Rates" section (this chapter) to estimate sediment mass accumulation rates (MARs). The average values of percentages of $CaCO_3$, C_{org}, linear sedimentation rate (LSR), dry bulk density (DBD), bulk-sediment mass accumulation rate (bulk MAR), $CaCO_3$ MAR, non-$CaCO_3$ MAR, and C_{org} MAR for 27 time intervals since 7.5 Ma are listed in Table 12. The mean values are presented vs. composite depth in Figure 27 and vs. age in Figure 28. Superimposed on the mean values are estimates of the instantaneous MAR calculated for each sample. The mean accumulation rates of bulk sediment are significantly lower than at any of the equatorial sites. Instead of the characteristic and well-defined maximum in MAR in the period from 7 to 4 Ma that was observed at the other sites, MARs at Site 853 appear to have declined steadily since 8 Ma. Upper Pliocene and Pleistocene carbonate accumulation rates are, on average, a factor of 4 lower than rates in the upper Miocene and lower Pliocene.

Gas Geochemistry

One sample for gas analysis was taken from each core of Hole 853B. We measured no hydrocarbon gas above detection limits.

PHYSICAL PROPERTIES

Introduction

Physical properties measured in whole-round samples for cores recovered at Site 853 included GRAPE bulk-density, compressional-wave velocity (using the multisensor track, MST), and thermal conductivity. Measurements in split-cores included (1) index properties: wet-bulk density, dry-bulk density, water content, and porosity; (2) compressional-wave velocity using the digital sonic velocimeter; and (3) vane shear strength using the Wykeham-Farrance vane shear device. In Hole 853B, we measured index properties, compressional-wave velocity, and vane-shear-strength twice per section. Thermal conductivity was measured at three locations (Sections 1, 3, and 5) per core in Hole 853B. In Hole 853C, compressional-wave velocities and index properties were measured once each section. Index property measurements were always taken at the same depth interval as the velocity measurements.

Index Properties

Wet-bulk density (Fig. 29; Table 13, CD-ROM, back pocket) ranges from 1.33 to 1.56 g/cm^3, grain density (Fig. 30) from 2.62 to 2.84 g/cm^3, porosity (Fig. 31) from 70% to 88%, and the water content (Fig. 32) from 86.5% to 258.8%. Both the porosity and the water content decrease with depth, while wet-bulk density increases with depth. The interval between 14 and 28 mbsf is significantly different from the mean in each of the downhole trends. In addition, the wet-bulk density, porosity, and water profiles are highly variable between 35 and 55 mbsf.

Table 6. Reversal boundary depths from Site 853.

Interval (cm)	Depth (mbsf)	Depth (mcd)	Interpretation	Age (Ma)	Comments
138-853A-1H-2, 125	2.70	2.80	Brunhes/Matuyama	0.73	
138-853A-1H-3, 75	3.75	3.85	Jaramillo (t)	0.91	
138-853A-1H-3, 110	4.10	4.20	Jaramillo (o)	0.98	
138-853A-1H-4, 35	4.85	4.95	Cobb Mountain (center)	1.10	
138-853A-1H-6, 25	7.75	7.85	Olduvai (t)	1.66	
138-853A-1H-6, 95	8.45	8.55	Olduvai (o)	1.88	
138-853B-1H-2, 140	2.90	2.90	Brunhes/Matuyma	0.73	
138-853B-1H-3, 85	3.85	3.85	Jaramillo (t)	0.91	
138-853B-3H-3, 60	7.90	7.85	Olduvai (t)	1.66	
138-853B-2H-3, 140	8.70	8.65	Olduvai (o)	1.88	
138-853B-2H-6, 40	12.20	12.15	Matuyama/Gauss	2.47	
138-853B-3H-1, 100	13.30	15.70	Kaena (o)	2.99	
138-853B-3H-2, 10	13.90	16.30	Mammoth (t)	3.08	
138-853B-3H-2, 65	14.45	16.85	Mammoth (o)	3.18	
138-853B-3H-3, 135	16.65	19.05	Gauss/Gilbert	3.40	
138-853B-3H-6, 10	19.90	22.30	Cochiti (t)	3.88	
138-853B-4H-2, 75	22.55	23.55	Cochiti (o)	3.97	
138-853B-4H-3, 85	24.15	25.15	Nunivak (t)	4.10	
138-853B-4H-4, 25	25.05	26.05	Nunivak (o)	4.24	
138-853B-4H-4, 150	26.30	27.30	Sidufjall (t)	4.40	Section break
138-853B-4H-5, 75	27.05	28.05	Sidufjall (o)	4.47	
138-853B-4H-6, 10	27.90	28.90	Thveral (t)	4.57	
138-853B-5H-5, 70	35.00	38.45	C3A-nl (t)	5.35	
138-853B-6H-2, 50	39.80	43.60	C3A-n2 (t)	5.68	
138-853B-6H-4, 40	42.70	46.50	C3A-n2 (o)	5.89	
138-853B-7H-2, 120	50.00	54.15	C3A-n3 (o)	6.50	
138-853B-7H-3, 110	51.40	55.55	C4-nl (t)	6.70	
138-853B-7H-4, 35	52.15	56.30	R-GTN		
138-853B-7H-4, 60	52.50	56.55	N-GTR		
138-853B-7H-5, 85	54.15	58.30	C4-nl (o)	6.78	
138-853B-7H-5, 150	54.80	58.85	C4-n2 (t)	6.85	Section break
138-853C-1H-2, 60	1.97	3.07	B/M	0.73	
138-853C-1H-2, 145	2.82	3.92	Jaramillo (t)	0.91	Section break
138-853C-1H-3, 30	3.17	4.27	Jarmaillo (o)	0.98	
138-853C-1H-3, 105	3.92	5.02	Cobb Mountain (center)	1.10	
138-853C-1H-5, 80	6.67	7.77	Olduvai (t)	1.66	
138-853C-1H-6, 05	7.47	8.57	Olduvai (o)	1.88	
138-853C-2H-1, 80	9.80	12.20	Matuyama/Gauss	2.47	
138-853C-2H-3, 85	12.85	15.25	Kaena (t)	2.92	
138-853C-2H-3, 135	13.35	15.75	Keana (o)	2.99	
138-853C-2H-4, 45	13.95	16.35	Mammoth (t)	3.08	
138-853C-2H-4, 100	14.45	16.85	Mammoth (o)	3.18	
138-853C-2H-5, 135	16.35	18.75	Gauss/Gilbert	3.40	
138-853C-3H-1, 150	19.90	23.40	Cochiti (o)	3.97	Section break
138-853C-3H-3, 20	21.70	25.20	Nunivak (t)	4.10	
138-853C-3H-3, 100	22.50	26.00	Nunivak (o)	4.24	
138-853C-3H-5, 15	24.65	28.15	Siddufjall (o)	4.47	
138-853C-3H-5, 100	25.50	29.00	Thvera (t)	4.57	
138-853C-4H-5, 105	33.55	38.70	C3A-nl (t)	5.35	
138-853C-5H-1, 90	38.40	43.45	C3A-n2 (t)	5.68	
138-853C-5H-3, 120	41.70	46.75	C3A-n2 (o)	5.89	
138-853C-6H-2, 90	49.40	55.45	C4-nl (t)	6.70	
138-853C-6H-3, 15	50.15	56.20	R-GTN		
138-853C-6H-3, 40	50.40	56.45	N-GTR		
138-853C-6H-4, 90	52.40	58.45	C4-nl (o)	6.78	
138-853C-6H-4, 140	52.90	59.05	C4-n2 (t)	6.85	
138-853D-1H-2, 125	2.75	2.95	B/M	0.73	
138-853D-1H-3, 65	3.65	3.85	Jaramillo (t)	0.91	
138-853D-1H-3, 100	4.00	4.20	Jarmaillo (o)	0.98	
138-853D-1H-6, 10	7.60	7.80	Olduvai (t)	1.66	Section break
138-853D-1H-6, 85	8.35	8.55	Olduvai (o)	1.88	
138-853D-2H-1, 90	9.70	12.20	Matuyama/Gauss	2.47	
138-853D-2H-3, 90	12.70	15.20	Kaena (t)	2.92	
138-853D-2H-3, 140	13.20	15.70	Kaena (o)	2.99	Section break
138-853D-2H-4, 45	13.75	16.25	Mammoth (t)	3.08	
138-853D-2H-4, 105	14.35	16.85	Mammoth (o)	3.18	
138-853D-2H-5, 130	16.00	18.50	Gauss/Gilbert	3.40	
138-853D-3H-1, 95	19.25	23.80	Cochiti (o)	3.88	
138-853D-3H-2, 100	20.80	25.35	Nunivak (t)	3.97	
138-853D-3H-3, 35	21.65	26.20	Nunivak (o)	4.10	
138-853D-3H-4, 15	22.95	27.50	Sidufjall (t)	4.24	
138-853D-3H-4, 90	23.70	28.25	Sidufjall (o)	4.40	
138-853D-3H-5, 10	24.40	28.95	Thvera (t)	4.47	Section break
138-853D-3H-6, 115	26.95	31.50	Thvera (o)	4.57	
138-853D-4H-5, 60	34.40	38.55	C3A-nl (t)	5.35	
138-853D-5H-2, 40	39.20	43.60	C3A-n2 (t)	5.68	
138-853D-5H-4, 40	42.20	46.60	C3A-n2 (o)	5.89	
138-853D-6H-1, 140	48.20	54.30	C3A-n3 (o)	6.50	Section break
138-853D-6H-3, 10	49.90	56.00	C4-nl (t)	6.70	
138-853D-6H-3, 50	50.30	56.40	R-GTN		Poorly defined
138-853D-6H-3, 9	50.70	56.80	N-GTR		Poorly defined
138-853D-6H-4, 110	52.40	58.50	C4-nl (o)	6.78	Poorly defined
138-853D-6H-5, 20	53.00	59.10	C4-n2 (t)	6.85	
138-853D-7H-2, 40	58.20	65.60	C4-n2 (o)	7.28	
138-853D-7H-4, 20	61.00	68.40	C4-n3 (t)	7.35	
138-853D-7H-4, 80	61.60	69.00	C4-n3 (o)	7.41	
138-853D-1H-2, 130	2.80	2.90	Brunhes/Matuyama	0.73	
138-853D-1H-3, 70	3.70	3.80	Jaramillo (t)	0.91	
138-853D-1H-3, 100	4.00	4.10	Jaramillo (o)	0.98	
138-853D-1H-4, 125	4.75	4.85	Cobb Mountain (center)	1.10	
138-853D-1H-6, 20	7.70	7.80	Olduvai (t)	1.66	
138-853D-2H-2, 130	11.30	12.20	Matuyama/Gauss	2.47	
138-853D-2H-4, 135	14.35	15.25	Kaena (t)	2.92	
138-853D-2H-5, 040	14.90	15.80	Kaena (o)	2.99	
138-853D-2H-5, 100	15.50	16.40	Mammoth (t)	3.08	
138-853D-2H-6, 10	16.10	17.00	Mammoth (o)	3.18	
138-853D-2H-7, 055	18.05	18.95	Gauss/Gilbert	3.40	

(t) = termination; (o) = onset.

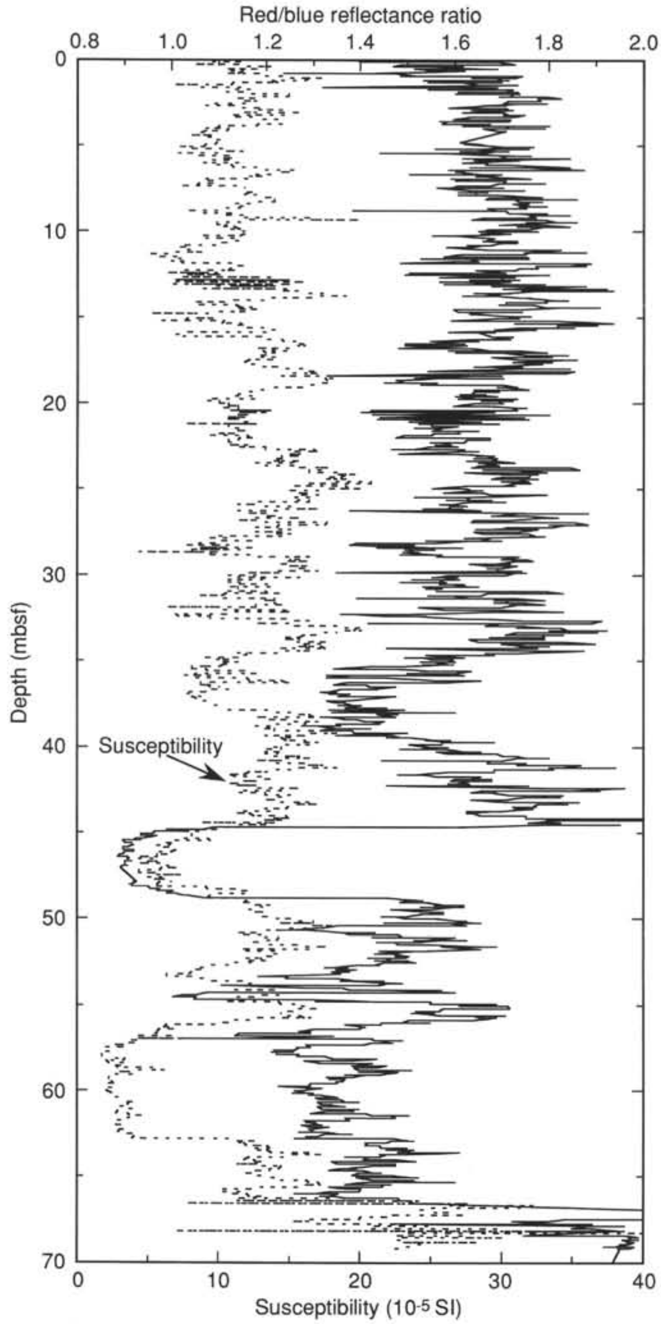

Figure 17. Relationship between the color changes (characterized by the red reflectance/blue reflectance ratio solid line) in the sediment from Hole 853C and the variations in the amount of magnetic material as expressed by the susceptibility variations (dashed line).

Compressional-Wave Velocity

Compressional-wave velocity (Fig. 33; Table 14, CD-ROM, back pocket) was measured perpendicular to bedding and ranges from 1493 to 1517 m/s. No downhole trend was apparent in the data sets. At the base of Hole 853C, the compressional-wave velocity is higher than that at the base of Hole 853B. Wet-bulk density is also higher and porosity lower than in Hole 853B. If we use composite depths for Holes 853B and 853C, the last physical property measurement for Hole 853C was taken almost 1.5 m below the last measurement in Hole 853B.

Table 7. Depths of top and bottom of each core in Site 853 in the composite depth section.

Core	ODP depth (mbsf)	Length (m)	Composite depth (mcd)	Delta (m)
138-853A-1H	0–10.15	10.15	0.10–10.25	0.10
138-853B-1H	0–4.25	4.25	0.00–4.25	0.00
138-853B-2H	4.30–14.11	9.81	4.25–14.06	–0.05
138-853B-3H	12.30–21.60	9.30	14.70–24.00	2.40
138-853B-4H	20.30–28.89	8.59	21.30–29.89	1.00
138-853B-5H	28.30–38.17	9.87	31.75–41.62	3.45
138-853B-6H	37.80–47.53	9.73	41.60–51.33	3.80
138-853B-7H	47.30–57.26	9.96	51.45–61.41	4.15
138-853B-8H	56.80–66.80	10.00	62.05–72.05	5.25
138-853B-9H	66.30–72.47	6.17	72.25–78.42	5.95
138-853C-1H	0.00–9.06	9.06	1.10–10.16	1.10
138-853C-2H	9.00–19.07	10.07	11.40–21.47	2.40
138-853C-3H	18.50–28.43	9.93	22.00–31.93	3.50
138-853C-4H	28.00–37.51	9.51	33.15–42.66	5.15
138-853C-5H	37.50–47.53	10.03	42.55–52.58	5.05
138-853C-6H	47.00–56.60	9.60	53.05–62.65	6.05
138-853C-7H	56.50–66.60	10.10	63.35–73.45	6.85
138-853C-8H	66.00–67.27	1.27	72.55–73.82	6.55
138-853D-1H	0.00–8.81	8.81	0.20–9.01	0.20
138-853D-2H	8.80–18.58	9.78	11.30–21.08	2.50
138-853D-3H	18.30–28.34	10.04	22.85–32.89	4.55
138-853D-4H	27.80–37.85	10.05	31.95–42.00	4.15
138-853D-5H	37.30–47.32	10.02	41.70–51.72	4.40
138-853D-6H	46.80–56.86	10.06	42.90–62.96	6.10
138-853D-7H	56.30–66.35	10.05	63.70–73.75	7.40
138-853E-1H	0.00–8.48	8.48	0.10–8.58	0.10
138-853E-2H	8.50–18.53	10.03	9.40–19.43	0.90

Table 8. Control points for sedimentation rates.

Composite depth (mcd)	Sediment. rate (m/m.y.)	Age (Ma)	Remarks
0		0.0	Core top
	4.04		
2.95		0.73	B *Brunhes Chron*
	5.0		
3.85		0.91	T *Jaramillo Subchron*
	4.86		
4.19		0.98	B *Jaramillo Subchron*
	6.25		
4.94		1.1	Cobb Mountain
	5.11		
7.8		1.66	T *Oldubai Subchron*
	3.51		
8.57		1.88	B *Oldubai Subchron*
	6.12		
12.18		2.47	B *Matuyama Chron*
	6.78		
15.23		2.92	T *Kaena Subchron*
	7.29		
15.74		2.99	B *Kaena Subchron*
	6.56		
16.33		3.08	T *Mammoth Subchron*
	5.60		
16.89		3.18	B *Mammoth Subchron*
	8.68		
18.8		3.4	B *Gauss Chron*
	7.29		
22.3		3.88	T *Cochiti Subchron*
	13.67		
23.53		3.97	B *Cochiti Subchron*
	13.08		
25.23		4.1	T *Nunibak Subchron*
	6.07		
26.08		4.24	B *Nunibak Subchron*
	8.37		
27.42		4.4	T *Sidujfall Subchron*
	10.43		
28.15		4.47	B *Sidujfall Subchron*
	8.0		
28.95		4.57	T *Thvera Subchron*
	12.75		
31.5		4.77	B *Thvera Subchron*
	12.19		
38.57		5.35	T *C3A–1*
	15.09		
43.55		5.68	T *C3A–2*
	14.14		
46.52		5.89	B *C3A–2*
	12.51		
54.15		6.5	B *C3A–3*
	13.94		
59.03		6.85	T *C4A–2*
	15.28		
65.6		7.28	B *C4A–2*
	8.95		
67.57		7.5	B *Discoaster berggreni*

T = top; B = bottom.

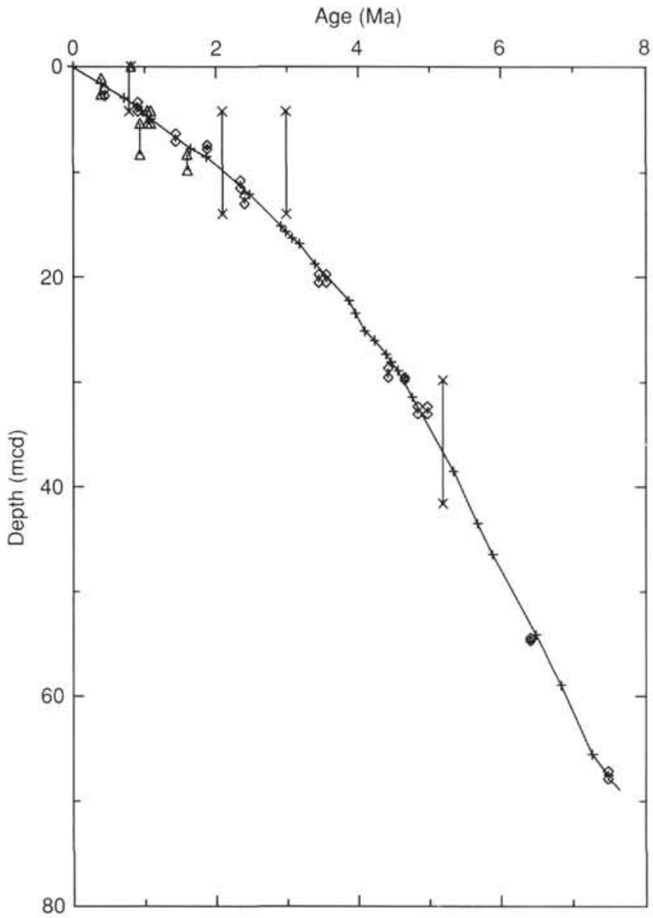

Figure 19. Plot of age vs. depth for Site 853 based on the calibration points in Table 8, compared with the nannofossil (diamonds), foraminifer (crosses), and radiolarian (triangles) datums. Age control points from Table 8 are indicated by crosses. For each datum the depth limits within which it was observed are indicated; where only a single symbol is visible the limits were too close to indicate at this plot scale.

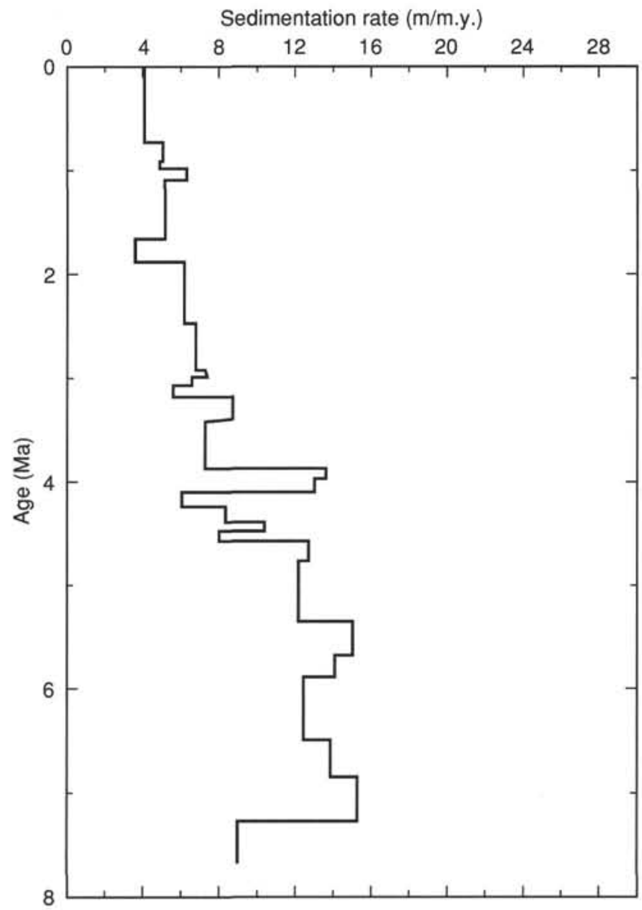

Figure 20. Linear sedimentation rate vs. age, based on the data in Table 8.

Thermal Conductivity

Thermal conductivity (Fig. 34; Table 15, CD-ROM, back pocket) is highly variable downhole and ranges from 0.86 to 1.21 W/(m • K). Because thermal conductivity is a function of the density and water content of the sediment, the thermal conductivity profile is similar to those index properties and is also marked by anomalously low values between 14 and 28 mbsf.

Shear Strength

Vane shear strength (Fig. 35; Table 16, CD-ROM, back pocket) values range between 9.6 and 68.5 kPa and generally increase with depth. Superimposed on this downhole trend are two sharp offsets in strength values. At both 28 and 44 mbsf, shear strength is offset by 32 kPa.

Relationships of Physical Properties to Lithology

The results from Site 853 indicate that the downhole distribution in physical properties is controlled by gravitational compaction with variations related to changes in carbonate and clay content superimposed on this trend. The calcareous sediments have higher wet-bulk density, grain density, and thermal conductivity and lower water content and porosity than the clay-rich sediments. For example, low wet-bulk densities (and high porosity and water content) in the interval from 14 to 28 mbsf result from clay-rich sediments, while several distinct interbeds of calcareous sediments (almost 90% nannofossils) found between 35 and 35 mbsf, 44 and 48 mbsf, and 56 and 66 mbsf have high wet-bulk densities (and lower porosity and water content) (Fig. 36).

SEISMIC STRATIGRAPHY

Modeling Procedure

Synthetic seismograms were generated from velocity and density models for Site 853 in order to correlate reflectors in the seismic section to stratigraphic changes. Due to the thin sediment cover at this site, no downhole logging was done. The density model was created by using laboratory densities only. Over the interval from 0 to 69.1 mbsf, a 10-point boxcar-filtered GRAPE density from Hole 853B was used. A constant value of 1.40 g/cm^3, equal to the value at 69.1 mbsf, was used for the interval 69.1–72.4 mbsf.

The velocity model was created using laboratory velocity collected with the DSV that were corrected to *in-situ* conditions for changes of sound speed as a function of temperature and pressure for the interval from 0 to 66.1 mbsf. The temperature gradient and bottom water temperature from Site 849 were used for these corrections. A constant value of 1500 m/s, equal to the velocity value at 66.1 mbsf, was used for the interval from 66.1 to 72.4 mbsf.

The accuracy of the traveltime-to-depth conversion was evaluated by the generation of synthetic seismograms and subsequent comparison to the seismic record collected over the site. Synthetic seismograms were generated using the above merged velocity and density

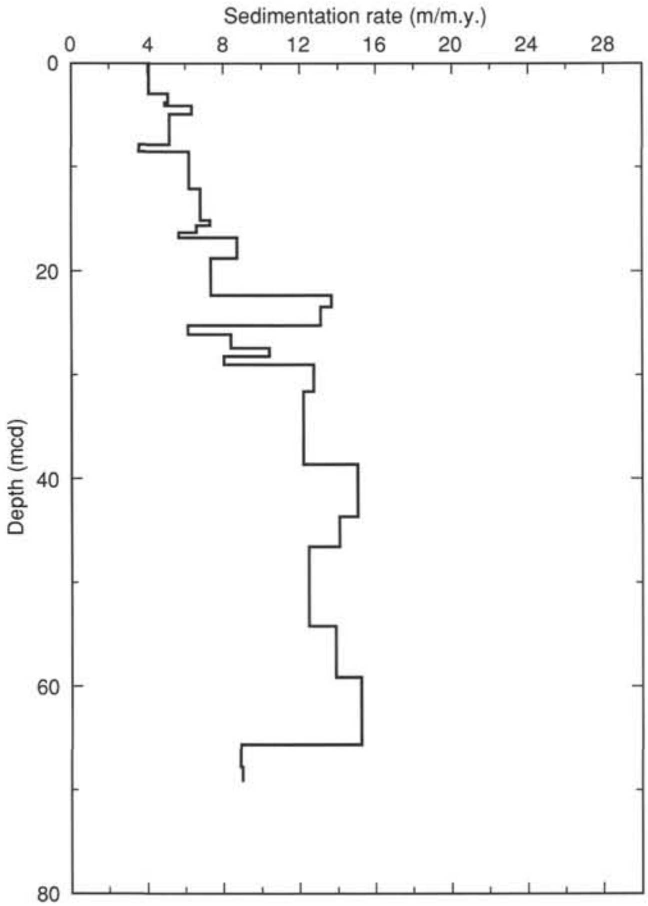

Figure 21. Linear sedimentation rate vs. composite depth, based on the data in Table 8.

data. These data were re-sampled at a 1-ms sample interval (~60 cm) and then used to calculate acoustic impedance and reflection coefficients and, finally, a synthetic seismogram. Density and velocity values typical of basalt (2.5 g/cm^3 and 3000 m/s, respectively) were added at the basement depth (72.4 mbsf) to generate a basement reflector in the synthetic. The model used to generate the synthetic seismogram has the same assumptions as described in previous site chapters (also, see Mayer et al., 1985). The final synthetic seismogram was filtered from 70 to 250 Hz., the same filter parameters as the field record collected at Site 853.

Results

A comparison of the synthetic seismogram with the seismic profile collected at Site 853 shows a good match between the two (Fig. 37). There is virtually a one-to-one correspondence between reflectors with an excellent match at basement. This suggests that the traveltime-to-depth conversion is fairly accurate.

Given an acceptable velocity model, the origin of some of the reflectors at Site 853 can be analyzed. As before, it must be emphasized that these are preliminary results that will undoubtedly be modified after more careful analysis. Eight major reflectors or reflector packages were identified. These reflectors were selected on the basis of amplitude and lateral coherency in the seismic record in the immediate area of Site 853. The two-way traveltime of the top and bottom of each reflector on the synthetic seismogram was measured, and by using the assumed velocity model, the depth range of each reflector was determined.

Within 1 m of the depth range of each major reflector, an associated change occurs in density (Fig. 38). Because little variation in velocity takes place with depth, changes in density are the sole cause of seismic reflections. The depths (synthetic, mbsf, and mcd) and ages (based on magnetostratigraphy and biostratigraphy of Site 853; see "Sedimentation Rates" section, this chapter) of these reflectors are presented in Table 17. A detailed understanding of the lithological, biostratigraphic, and ultimately, the paleoceanographic significance of these events must await shore-based studies at this time.

SUMMARY AND CONCLUSIONS

Site 853 was the sixth site drilled along the western transect of Leg 138. This transect, situated along 110° W, was designed to sample the various elements of the equatorial circulation system in an area far removed from the influence of the eastern boundary of the Pacific. The transect also serves as the eastern end-member of a series of studies (Legs 85 and 130) aimed at understanding the regional and global response of the equatorial Pacific Ocean to changes in climate. The present location of Site 853 is well within the eastward-flowing NECC. The site also seasonally underlies the Northern Hemisphere trade winds. The site was selected in a region where we thought that sediment rates were high enough so that we might see a record in both NECC fluctuations and trade winds.

Site 853 is located ~900 km west of the East Pacific Rise on crust generated ~10 Ma. The backtracked path of the site is straightforward and is constrained only by the movement of the Pacific Plate. Poles of rotation of the Pacific Plate have been estimated based on traces of hot spots (Duncan and Claque, 1985) and also by use of the age distribution of sediments from DSDP sites along the equatorial sediment bulge (van Andel et al., 1975; see Fig. 2 and Table 18). Neither of these reconstructions had Site 853 passing under the equatorial divergence.

From an original ridge crest depth of ~2800 m, Site 853 has subsided to its present depth of 3726 m and, in doing so, has intercepted a regionally and temporally variable lysocline. While five holes were drilled at Site 853, and the section is only ~73 m thick, severe ship's heave from bad weather resulted in several small gaps and a re-cored interval in the recovered section. As at other Leg 138 sites, we used real-time analyses of continuous core logs (GRAPE, susceptibility, and color reflectance) to monitor the offset between cores, but unfortunately the unpredictability of where the APC shoots in a heave cycle combined with the limits of time prevented us from recovering 100% of the section.

Basalt was recovered in Hole 853B when the APC bounced off basement at ~73 mbsf. Above basaltic basement is a continuous upper Miocene to Pleistocene sequence of clayey nannofossil oozes and nannofossil oozes having more abundant foraminifers and iron and manganese oxides in the upper 28 m (0–4.5 Ma). Reflecting the relatively low productivity due to the northern location of the site, siliceous microfossils are almost totally absent and are present only in the upper few meters (last 500–600 k.y.). The last few hundred thousand years were a time of the lowest sedimentation and accumulation rates (Fig. 39A) and a time at which Site 853 was farthest away from the equator. Interspersed within the section are several intervals of almost pure nannofossil ooze, marked by high carbonate content intervals (Fig. 39C), probably representative of times of enhanced carbonate preservation. The presence of siliceous microfossils only in the upper few meters may be the result of post-sedimentation processes, but this was not supported by the pore-water chemistry.

Stratigraphic control at Site 853 was provided mainly by nannofossils and an excellent magnetostratigraphy. All reversals from the Brunhes Chron to the top of Chron C4A were recognized and several small reversals not yet part of the magnetic polarity time scale have been identified. Susceptibility levels were relatively high throughout and played an important role in interhole correlations (Fig. 39B).

Table 9. Interstitial-water geochemical data for Holes 853A and 853B.

Core, section, interval (cm)	Depth (mbsf)	pH	Salinity	Chloride (mM)	Sodium (mM)	Alkalinity (mM)	Sulfate (mM)	Magnesium (mM)	Calcium (mM)	Potassium (mM)	Strontium (μM)	Lithium (μM)	Silica (μM)	Ammonia (μM)
138-835A-1H-1, 141-150	1.5	7.53	35.5	557	478	2.796	28.02	52.87	10.41	11.2	89	26.6	451	<10
853A-1H-5, 145-150	7.5	7.52	36.2	557	477	2.646	28.11	53.23	10.53	11.3	92	32.6	545	<10
853B-2H-5, 145-150	11.8	7.56	36.0	556	476	2.719	28.16	53.39	10.68	10.9	92	32.3	443	<10
853B-3H-6, 145-150	21.3	7.55	36.0	559	479	2.645	27.94	53.33	10.66	10.9	93	32.6	349	<10
853B-4H-6, 145-150	26.3	7.58	36.0	558	478	2.628	28.24	53.47	10.61	11.0	94	32.7	330	<10
853B-5H-6, 135-140	37.2	7.61	36.3	557	475	2.593	27.34	53.68	10.47	10.6	90	33.1	315	<10
853B-6H-5, 145-150	45.3	7.55	36.3	557	476	2.547	27.57	53.82	10.42	10.5	91	33.4	383	<10
853B-7H-6, 145-150	56.3	7.57	36.3	558	478	2.477	27.64	53.66	10.34	10.3	90	33.6	454	<10
853B-8H-6, 145-150	65.8	7.62	36.0	556	477	2.425	27.54	53.00	10.27	10.4	86	32.7	473	<10

Sedimentation rates were low at Site 853, and the general shape of the sedimentation rate curve (Fig. 39A) differed from that of the previous western transect sites in that it showed a general decrease from the late Miocene to the Pleistocene, reflecting the northward movement of the site away from any influence of the equatorial current system. However, superimposed on this general trend were short intervals of increased and decreased sedimentation and accumulation rates that follow a pattern similar to that at other Leg 138 sites.

The first sediment to accumulate above the newly formed Site 853 was a nannofossil ooze that contained a substantial component of hydrothermally derived iron-oxides and clays. Initial sedimentation rates at the site probably were ~6 to 8 m/m.y (Fig. 39A), but are poorly constrained because of the absence of stratigraphic markers in this interval. Sedimentation rates increased to ~15 m/m.y. at ~7.5 Ma and stayed at this level until ~4.8 Ma. During the Pliocene and Pleistocene, sedimentation rates decreased to ~4 or 5 m/m.y. The sediment in this interval has a relatively high abundance of foraminifers.

The low organic carbon influx at Site 853 clearly is reflected in the interstitial-water chemistry, which suggests that, on a macro-scale, the sediment column at Site 853 has been oxidizing throughout. Alkalinity profiles suggest that dissolution has been confined to the sediment/water interface where oxygen and nitrate are being consumed to oxidize organic matter. With the relatively low sedimentation and organic carbon accumulation rates present at Site 853, all of the labile organic matter was consumed before burial.

Superimposed on these general long-term trends in sedimentation are high-frequency fluctuations in the ratios of carbonate and clay abundances. Sorting out the significance of these changes in terms of atmospheric circulation, surface circulation, and deep-water chemistry will be the subject of shore-based studies.

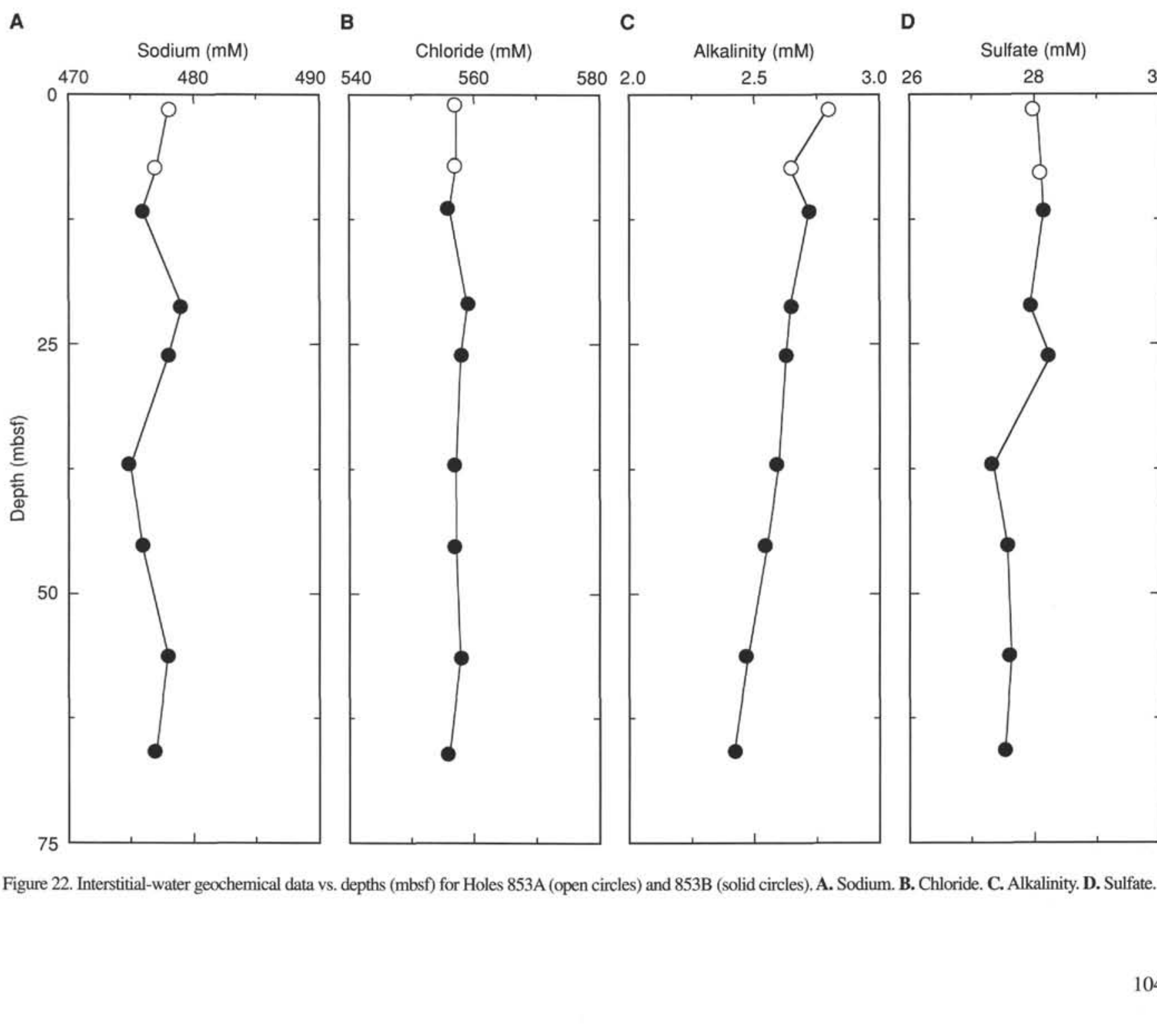

Figure 22. Interstitial-water geochemical data vs. depths (mbsf) for Holes 853A (open circles) and 853B (solid circles). **A.** Sodium. **B.** Chloride. **C.** Alkalinity. **D.** Sulfate.

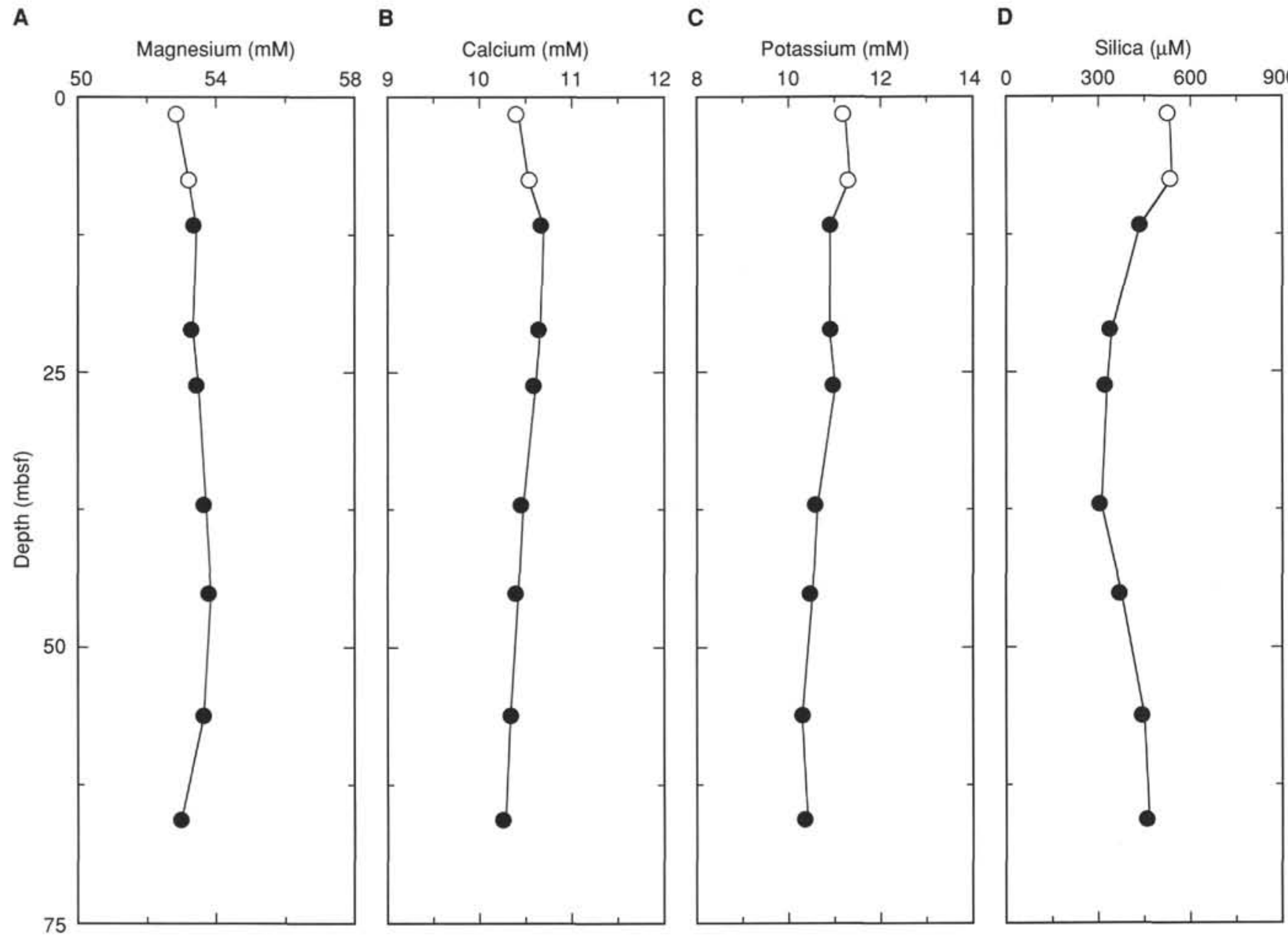

Figure 23. Interstitial-water geochemical data vs. depths (mbsf) for Holes 853A (open circles) and 853B (solid circles). **A.** Magnesium. **B.** Calcium. **C.** Potassium. **D.** Silica.

REFERENCES

Baker, P. A., 1986. Pore water chemistry of carbonate-rich sediments, Lord House Rise, Southwest Pacific Ocean. *In* Kennett, J. P., von der Borch, C. C. et al., *Init. Repts. DSDP,* 90: Washington (U.S. Govt. Printing Office), 1249–1256.

Duncan, R., and Claque, D., 1985. Pacific plate motion is recorded by linear volcanic chains. *In* Narin, A.E.M., Stehli, F. G., and Uyeda, U. (Eds.), *Ocean Basins and Margins,* Vol. 7A: New York (Plenum Pubs.), 89–121.

Froelich, P. N., Klinkhammer, G. P., Bender, M. L., Heath, G. R., Luedtke, N., Cullen, D., Daulphin, P., Hammond, D., Hartman, B., and Maynard, V., 1979. Early oxidation of organic matter in pelagic sediments of the Eastern Equatorial Atlantic: suboxic diagenesis. *Geochim. Cosmochim. Acta.,* 43:1075–1090.

Mammerickx, J., 1989. The Eastern Pacific Ocean and Hawaii, *In* Winterer, E. L., et al. (Eds.), *The Geology of North America,* Vol. N. Geol. Soc. Am., Plate 1C.

Martini, E. 1971. Standard Tertiary and Quaternary calcareous nannoplankton zonation. *Proc. 2nd Int. Conf. on Planktonic Microfossils, Roma 1970.* Rome (Ed. Tecnoscienza), 739–785.

Mayer, L. A., 1979. The origin of fine scale acoustic stratigraphy in deep-sea carbonates. *J. Geophys. Res.,* 804:6177–6184.

Mayer, L. A., Shipley, T. H. Theyer, F., Wilkens, R. W., and Winterer, E. L., 1985. Seismic modelling and paleoceanography at DSDP Site 574. *In* Mayer, L. A., Theyer, F., Thomas, E., et al., *Init. Repts. DSDP,* 85: Washington (U.S. Govt. Printing Office), 947–970.

Okada, H., and Bukry, D. 1980. Supplementary modification and introduction of code numbers to the low-latitude coccolith biostratigraphic zonation (Bukry, 1973; 1975). *Mar. Micropaleontol.,* 5:321–325.

Pedersen, T. F., and Shimmield, G. B., 1991. Interstitial water chemistry, Leg 117: Contrasts with the Peru Margin. *In* Prell, W. L., Niitsuma, N., et al., *Proc. ODP, Sci. Results,* 117: College Station, TX (Ocean Drilling Program), 499–513.

Suess, E., von Huene, R., et al., 1988. *Proc. ODP., Init. Repts.,* 112: College Station, TX (Ocean Drilling Program).

van Andel, T. H., Heath, G. R., and Moore, T. C., 1975. Cenozoic tectonics, sedimentation, and paleoceanography of the central equatorial Pacific. *Geol. Soc. Am. Mem.,* 143.

Ms 138A-118

NOTE: For all sites drilled, core description forms ("barrel sheets") and core photographs have been reproduced on coated paper and can be found in Section 8, beginning on page 1099. Forms containing smear-slide data can be found in Section 9, beginning on page 1435.

Formation microscanner images for this site are presented on microfiche in the back of Part 2.

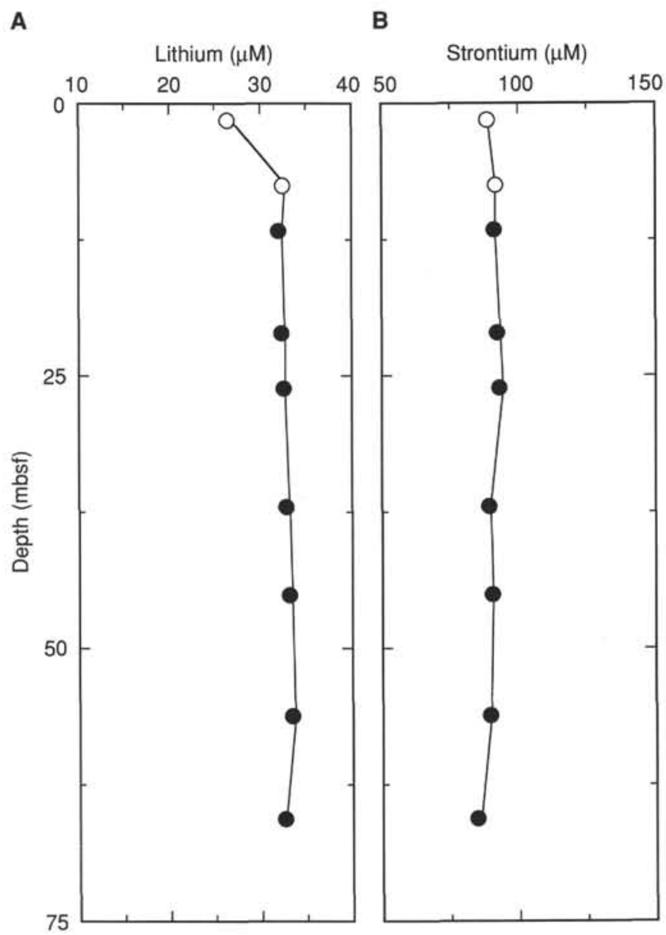

Figure 24. Interstitial-water geochemical data vs. depths (mbsf) for Holes 853A (open circles) and 853B (solid circles). **A.** Lithium. **B.** Strontium.

Table 11. Duplicate analyses of percentages of $CaCO_3$ in samples from Site 853.

Core, section, interval (cm)	ODP depth (mbsf)	Composite depth (mcd)	First run C_aCO_3 (%)	Second run C_aCO_3 (%)	Absolute value of C_aCO_3 (difference)
138-853B-					
1H-2, 102–104	2.53	2.53	79.21	79.46	0.25
2H-2, 102–104	6.83	6.78	63.99	64.58	0.59
2H-5, 102–104	11.33	11.28	82.93	81.74	1.18
2H-6, 33–35	12.14	12.09	65.51	64.25	1.27
2H-6, 102–104	12.83	12.78	80.39	80.14	0.25
3H-1, 43–45	12.74	15.14	55.62	55.71	0.08
3H-2, 113–115	14.94	17.34	74.90	74.56	0.34
3H-3, 102–104	16.33	18.73	39.98	41.00	1.01
3H-5, 33–35	18.64	21.04	41.59	40.91	0.68
4H-2, 103–105	22.84	23.84	53.93	53.34	0.59
4H-4, 103–105	25.84	26.84	80.98	79.55	1.44
5H-1, 113–115	29.44	32.89	61.96	64.16	2.20
5H-2, 102–104	30.83	34.28	74.14	73.80	0.34
5H-3, 102–104	32.33	35.78	88.34	87.66	0.68
5H-4, 33–35	33.14	36.59	51.82	50.72	1.10
6H-2, 102–104	40.33	44.13	75.66	72.61	3.04
6H-4, 102–104	43.33	47.13	65.60	65.18	0.42
6H-6, 42–44	45.73	49.53	90.11	89.69	0.42
7H-1, 102–104	48.33	52.48	70.42	71.42	1.01
7H-2, 102–104	49.83	53.98	72.78	73.29	0.51
7H-6, 42–44	55.23	59.38	61.20	59.17	2.03
7H-7, 28–30	56.59	60.74	87.90	87.07	0.17
8H-1, 102–104	57.83	63.08	89.10	89.27	0.17
8H-2, 97–99	59.28	64.53	84.20	83.69	0.51
Average					0.85

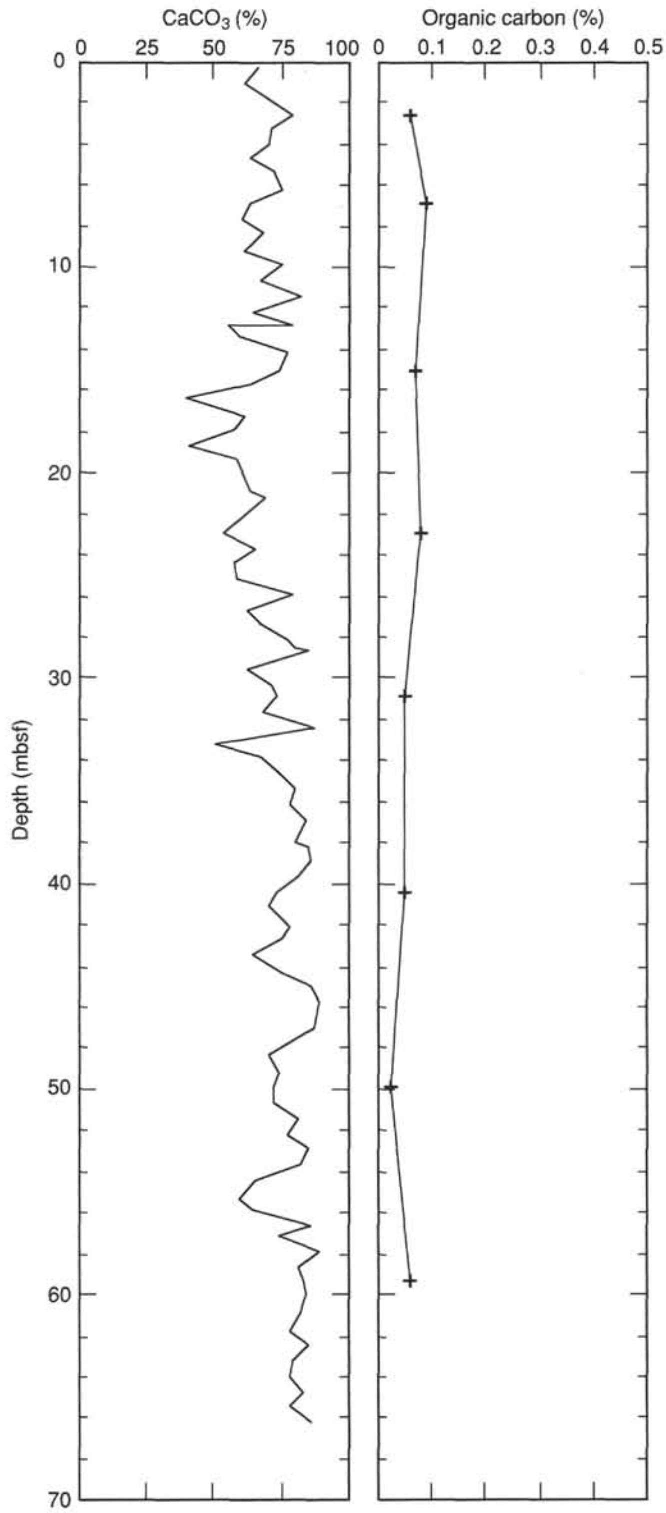

Figure 25. Downhole records of percentages of $CaCO_3$ and C_{org} vs. ODP depth (mbsf) for Site 853.

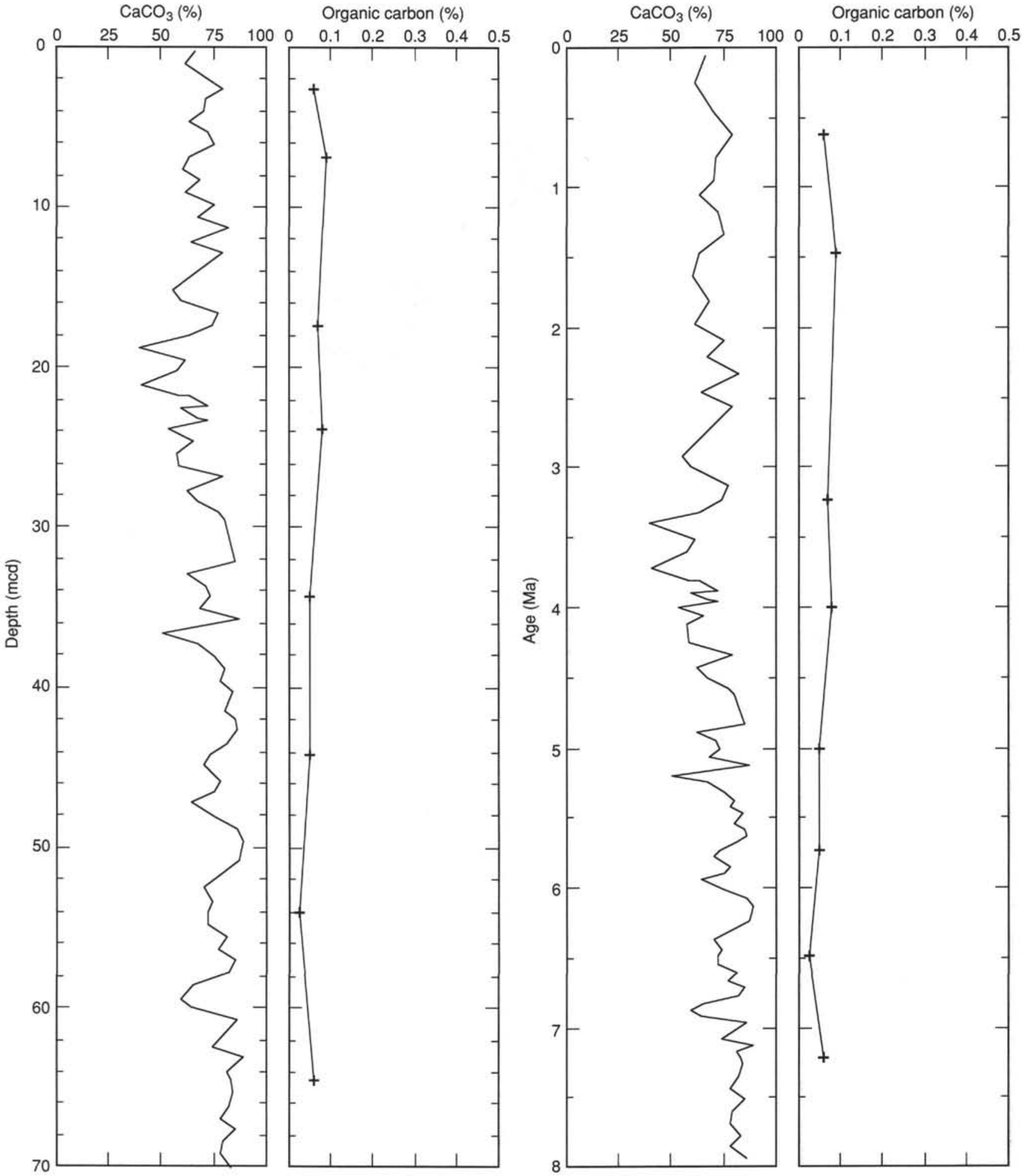

Figure 26. Plots of percentages of $CaCO_3$ and C_{org} vs. composite depth (mcd) and age for Site 853.

Table 12. Average values of sedimentary parameters calculated over time intervals defined by chronostratigraphic levels.

Composite depth (mcd)	Ag (Ma)	Mean C_aCO_3 (%)	Mean Corg (%)	Sed. rate (m/m.y.)	Mean DBD (g/cm^3)	Mean bulk MAR (g/cm^2/k.y.)	Mean C_aCO_3 MAR (g/cm^2/k.y.)	Mean non-C_aCO_3 MAR (g/cm^2/k.y.)	Mean Corg MAR (mg/cm^2/k.y.)
0	0								
		6.98	0.06	4.04	0.55	0.22	0.15	0.07	0.1
2.95	0.73								
		7.19		5.00	0.55	0.28	0.20	0.08	
3.85	0.91								
		7.06		4.86	0.53	0.26	0.18	0.08	
4.19	0.98								
		6.42		6.25	0.53	0.33	0.21	0.12	
4.94	1.10								
		68.4	0.09	5.11	0.49	0.25	0.17	0.08	0.2
7.80	1.66								
		69.1		3.50	0.45	0.16	0.11	0.05	
8.57	1.88								
		70.6		6.12	0.59	0.36	0.26	0.11	
12.18	2.47								
		68.0		6.78	0.58	0.39	0.27	0.13	
15.23	2.92								
		60.4		7.29	0.48	0.35	0.21	0.14	
15.74	2.99								
				6.56					
16.33	3.08								
		77.4		5.60	0.35	0.20	0.15	0.04	
16.89	3.18								
		59.7	0.07	8.68	0.40	0.35	0.21	0.14	0.2
18.80	3.40								
		56.7		7.29	0.47	0.34	0.19	0.15	
22.30	3.88								
		68.2		13.67	0.46	0.62	0.42	0.20	
23.53	3.97								
		59.9	0.08	13.08	0.43	0.56	0.33	0.22	0.4
25.23	4.10								
		58.5	6.07	6.07	0.45	0.27	0.16	0.11	
26.08	4.24								
		69.9		8.38	0.52	0.43	0.30	0.13	
27.42	4.40								
		62.9		10.43	0.37	0.39	0.24	0.14	
28.15	4.47								
		68.0		8.00	0.38	0.30	0.21	0.10	
28.95	4.57								
		79.1		12.75	0.63	0.80	0.63	0.17	
31.50	4.77								
		71.9	0.05	12.19	0.60	0.73	0.53	0.21	0.4
38.57	5.35								
		82.6		15.09	0.64	0.96	0.79	0.17	
43.55	5.68								
		75.0	0.05	14.14	0.71	1.00	0.75	0.25	0.5
46.52	5.89								
		79.2	0.03	12.51	0.65	0.82	0.65	0.17	0.2
54.15	6.50								
		77.5		13.94	0.62	0.86	0.67	0.19	
59.03	6.85								
		78.5	0.06	15.28	0.73	1.12	0.88	0.24	0.7
65.60	7.28								
		81.0		8.95	0.80	0.71	0.58		0.14
67.57	7.50								

DBD=dry-bulk density; MAR=mass accumulation rate.

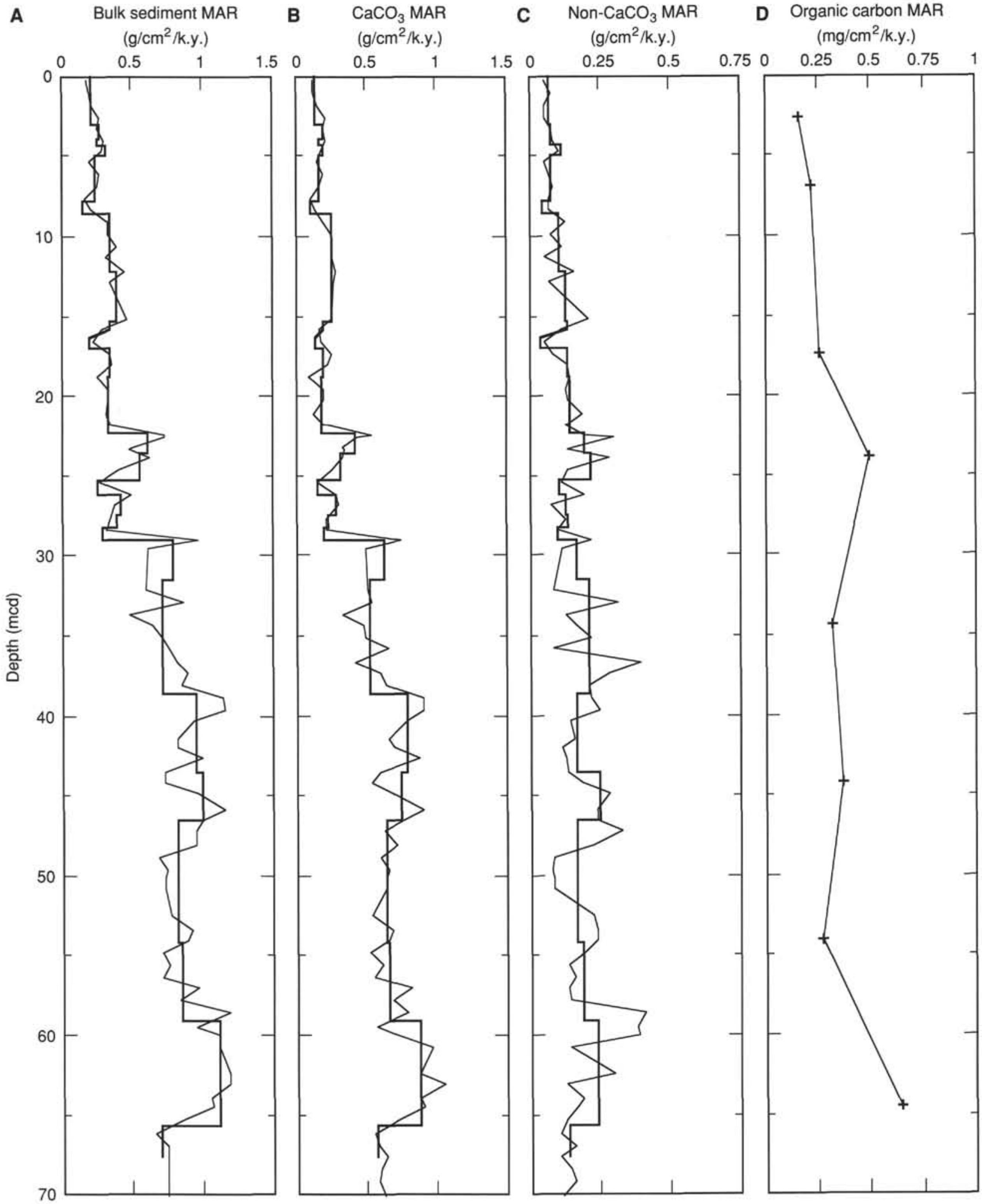

Figure 27. Mass accumulation rates of (**A**) bulk sediment, (**B**) $CaCO_3$, (**C**) non-$CaCO_3$, and (**D**) C_{org} vs. composite depth at Site 853. Note different units for C_{org}. Thick line indicates mean value between each stratigraphic datum plane. Thin line shows discrete accumulation rates calculated for each sample.

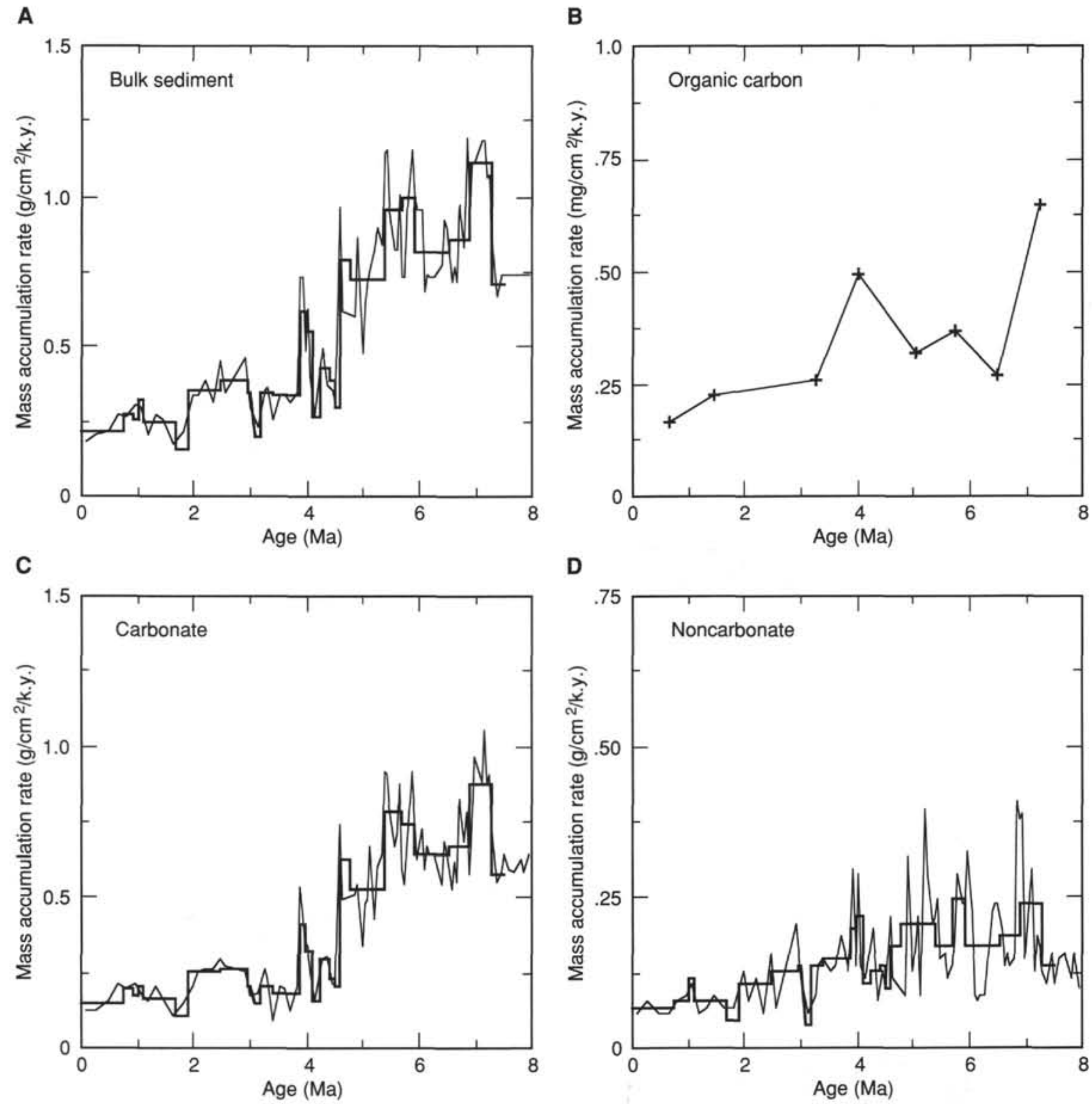

Figure 28. Mass accumulation rates of (**A**) bulk sediment, (**B**) C_{org}, (**C**) $CaCO_3$, (**D**) non-$CaCO_3$ vs. age in sediments from Site 853. Thick line indicates mean value between each stratigraphic datum plane. Thin line shows discrete accumulation rates calculated for each sample.

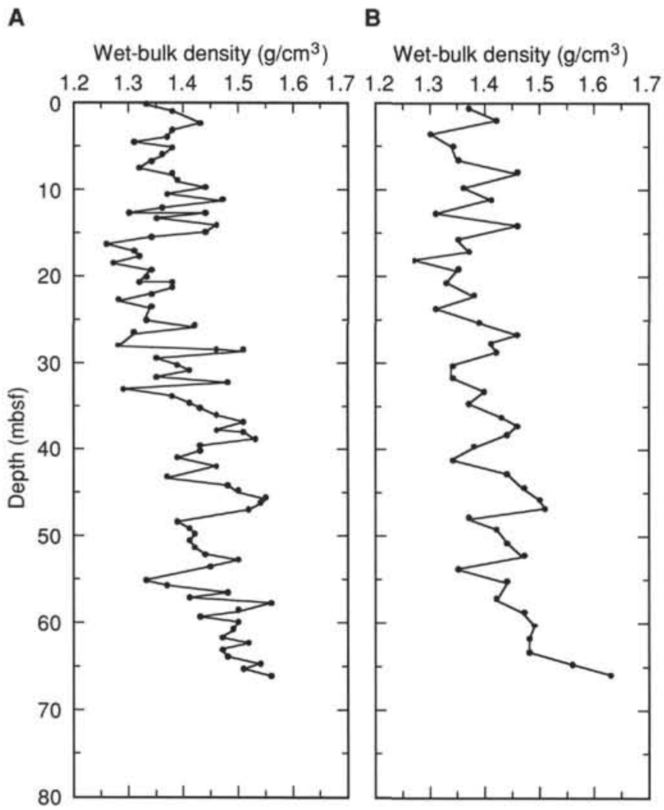

Figure 29. Wet-bulk density vs. depth for Holes 853B (**A**) and 853C (**B**).

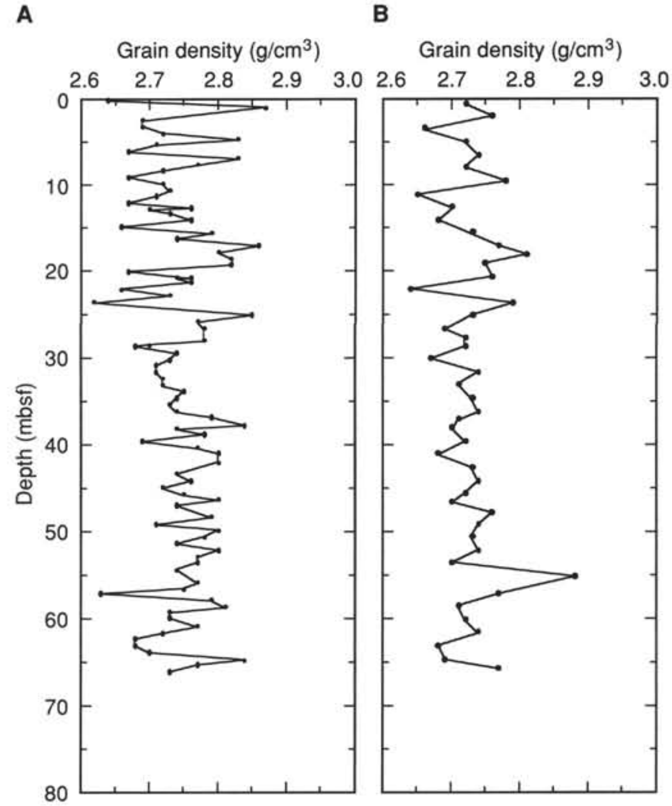

Figure 30. Grain density vs. depth for Holes 853B (**A**) and 853C (**B**).

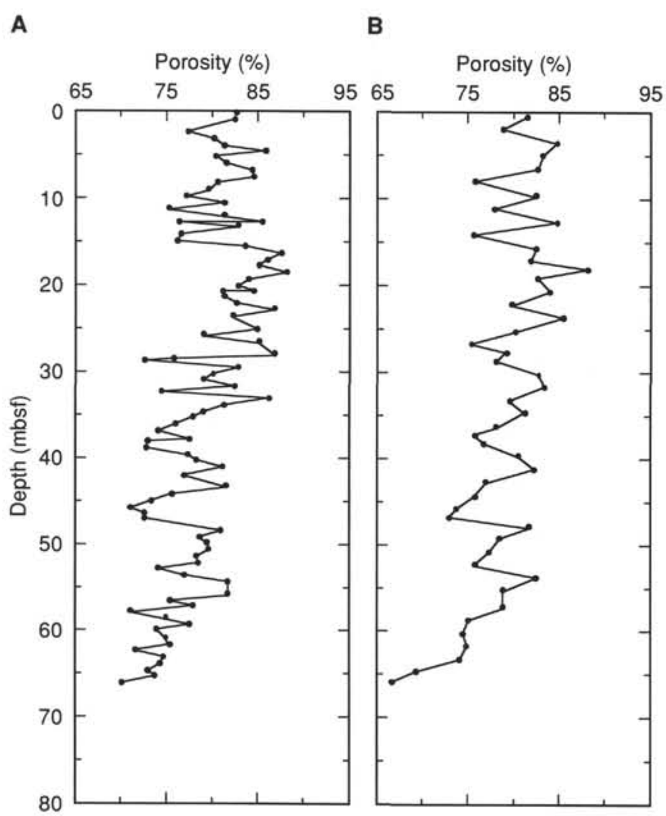

Figure 31. Porosity vs. depth for Holes 853B (**A**) and 853C (**B**).

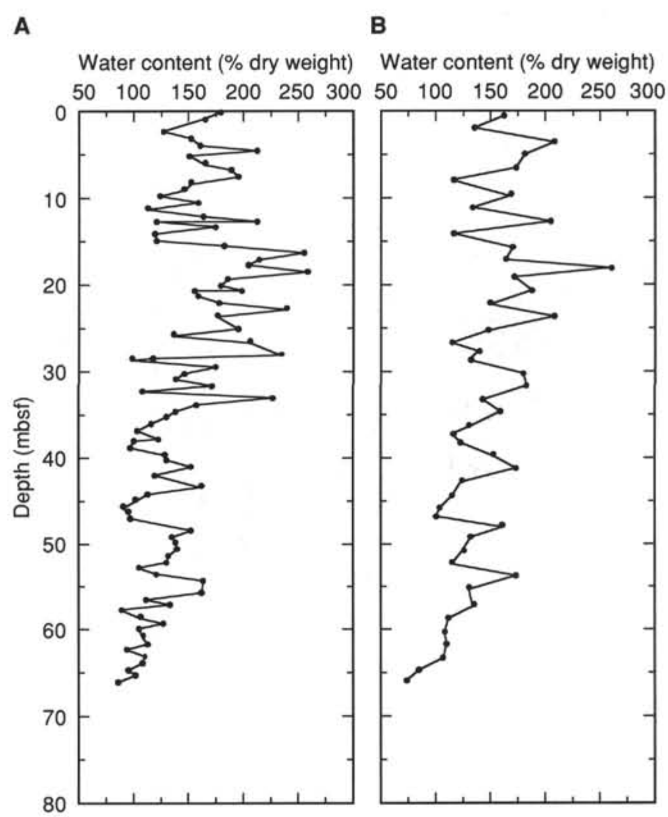

Figure 32. Water content vs. depth for Holes 853B (**A**) and 853C (**B**).

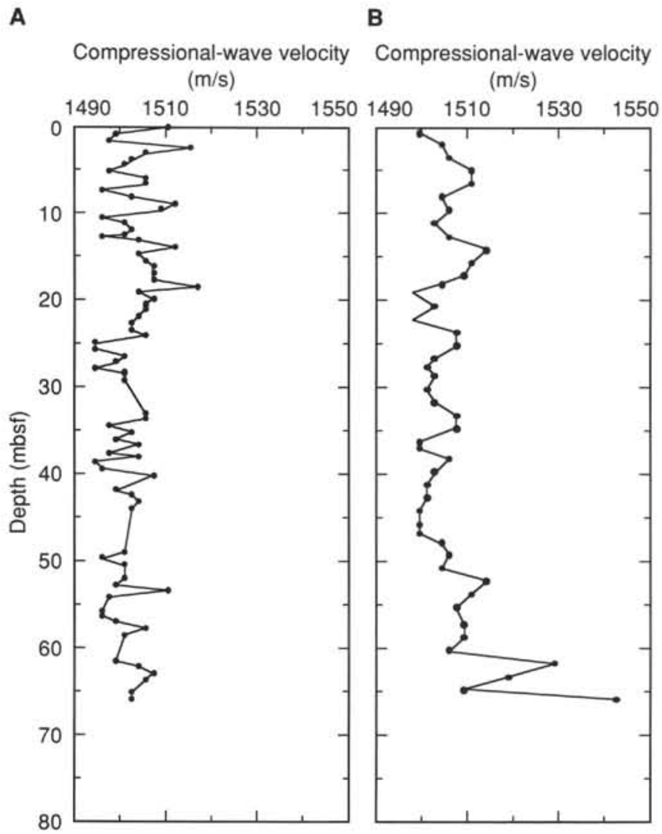

Figure 33. Velocity vs. depth for Holes 853B (**A**) and 853C (**B**).

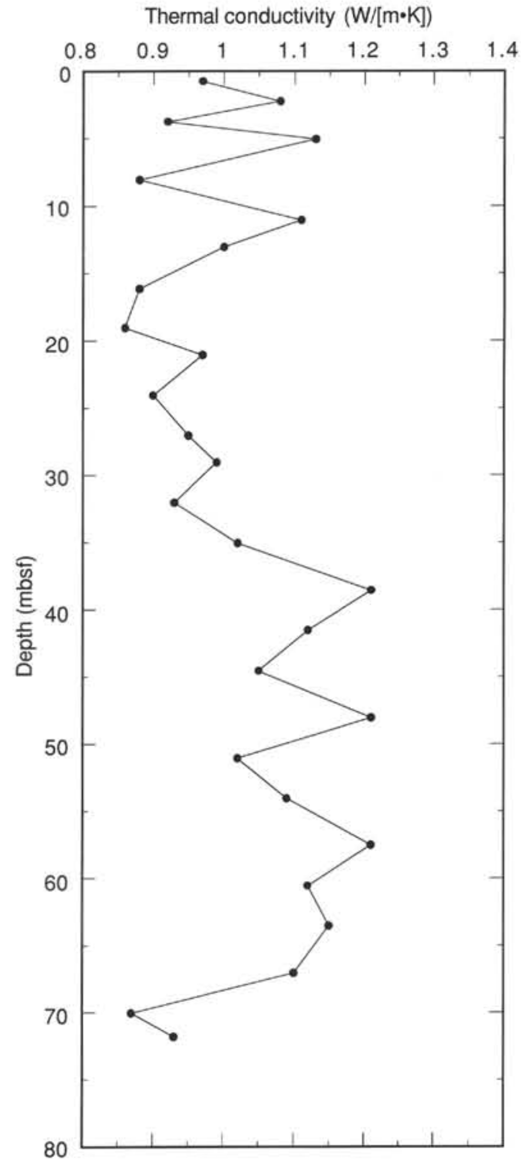

Figure 34. Thermal conductivity data vs. depth for Hole 853B.

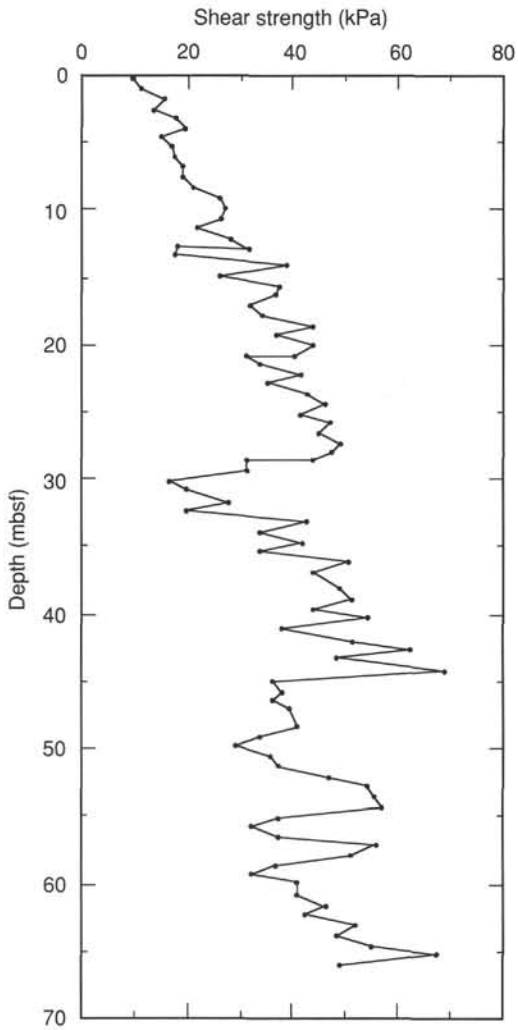

Figure 35. Undrained shear strength data vs. depth for Hole 853B.

Table 16. Vane shear strength data for Site 853.

Core, section, Interval (cm)	Depth (mbsf)	Depth (mcd)	Shear strength (kPa)
138-853B-			
1H-1, 23–23	0.23	0.23	9.6
1H-1, 103–103	1.03	1.03	11.4
1H-2, 33–33	1.83	1.83	15.9
1H-2, 103–103	2.53	2.53	13.6
1H-3, 22–22	3.22	3.22	17.9
1H-3, 102–102	4.02	4.02	19.7
2H-1, 33–33	4.63	4.58	15.0
2H-1, 103–103	5.33	5.28	17.3
2H-2, 33–33	6.13	6.08	17.9
2H-2, 103–103	6.83	6.78	19.3
2H-3, 33–33	7.63	7.58	19.1
2H-3, 103–103	8.33	8.28	21.1
2H-4, 33–33	9.13	9.08	26.0
2H-4, 103–103	9.83	9.78	27.2
2H-5, 33–33	10.63	10.58	26.4
2H-5, 103–103	11.33	11.28	21.9
2H-6, 33–33	12.13	12.08	27.8
3H-1, 43–43	12.73	15.13	18.0
2H-6, 103–103	12.83	12.78	31.5
3H-1, 103–103	13.33	15.73	17.6
3H-2, 33–33	14.13	16.53	38.7
3H-2, 113–113	14.93	17.33	26.1
3H-3, 33–33	15.63	18.03	37.4
3H-3, 103–103	16.33	18.73	36.9
3H-4, 33–33	17.13	19.53	32.0
3H-4, 103–103	17.83	20.23	34.2
3H-5, 33–33	18.63	21.03	43.7
3H-5, 103–103	19.33	21.73	36.9
3H-6, 33–33	20.13	22.53	43.7
4H-1, 43–43	20.73	21.73	31.5
3H-6, 103–103	20.83	23.23	40.1
4H-1, 103–103	21.33	22.33	33.8
4H-2, 33–33	22.13	23.13	41.5
4H-2, 103–103	22.83	23.83	35.1
4H-3, 33–33	23.63	24.63	42.4
4H-3, 103–103	24.33	25.33	46.0
4H-4, 33–33	25.13	26.13	41.5
4H-4, 103–103	25.83	26.83	46.9
4H-5, 33–33	26.63	27.63	44.6
4H-5, 103–103	27.33	28.33	48.7
4H-6, 23–23	28.03	29.03	47.3
4H-6, 73–73	28.53	29.53	43.7
5H-1, 34–34	28.64	32.09	31.5
5H-1, 114–114	29.44	32.89	31.5
5H-2, 44–44	30.24	33.69	16.7
5H-2, 104–104	30.84	34.29	19.8
5H-3, 34–34	31.64	35.09	27.9
5H-3, 103–103	32.33	35.78	19.8
5H-4, 34–34	33.14	36.59	42.4
5H-4, 103–103	33.83	37.28	33.8
5H-5, 34–34	34.64	38.09	41.5
5H-5, 103–103	35.33	38.78	33.8
5H-6, 34–34	36.14	39.59	50.5
5H-6, 103–103	36.83	40.28	43.7
6H-1, 34–34	38.14	41.94	48.8
6H-1, 103–103	38.83	42.63	51.0
6H-2, 34–34	39.64	43.44	43.7
6H-2, 103–103	40.33	44.13	53.9
6H-3, 23–23	41.03	44.83	37.9
6H-3, 126–126	42.06	45.86	51.0
6H-4, 33–33	42.63	46.43	62.0
6H-4, 103–103	43.33	47.13	48.1
6H-5, 44–44	44.24	48.04	68.5
6H-5, 114–114	44.94	48.74	36.5
6H-6, 44–44	45.74	49.54	37.9
6H-6, 104–104	46.34	50.14	36.5
6H-7, 20–20	47.00	50.80	39.4
7H-1, 104–104	48.34	52.49	40.8
7H-2, 34–34	49.14	53.29	33.5
7H-2, 104–104	49.84	53.99	29.2
7H-3, 34–34	50.64	54.79	35.7
7H-3, 104–104	51.34	55.49	37.2
7H-4, 34–34	52.14	56.29	46.7
7H-4, 104–104	52.84	56.99	53.9
7H-5, 29–29	53.59	57.74	55.4
7H-5, 109–109	54.39	58.54	56.9
7H-6, 42–42	55.22	59.37	37.2
7H-6, 103–103	55.83	59.98	32.1
7H-7, 28–28	56.58	60.73	37.2
8H-1, 34–34	57.14	62.39	55.4
8H-1, 104–104	57.84	63.09	51.0
8H-2, 34–34	58.64	63.89	36.5
8H-2, 98–98	59.28	64.53	32.1
8H-3, 14–14	59.94	65.19	40.8
8H-3, 105–105	60.85	66.10	40.8
8H-4, 42–42	61.72	66.97	45.9
8H-4, 105–105	62.35	67.60	42.3
8H-5, 33–33	63.13	68.38	51.8
8H-5, 114–114	63.94	69.19	48.1
8H-6, 46–46	64.76	70.01	54.7
8H-6, 103–103	65.33	70.58	67.1
8H-7, 33–33	66.13	71.38	49.0

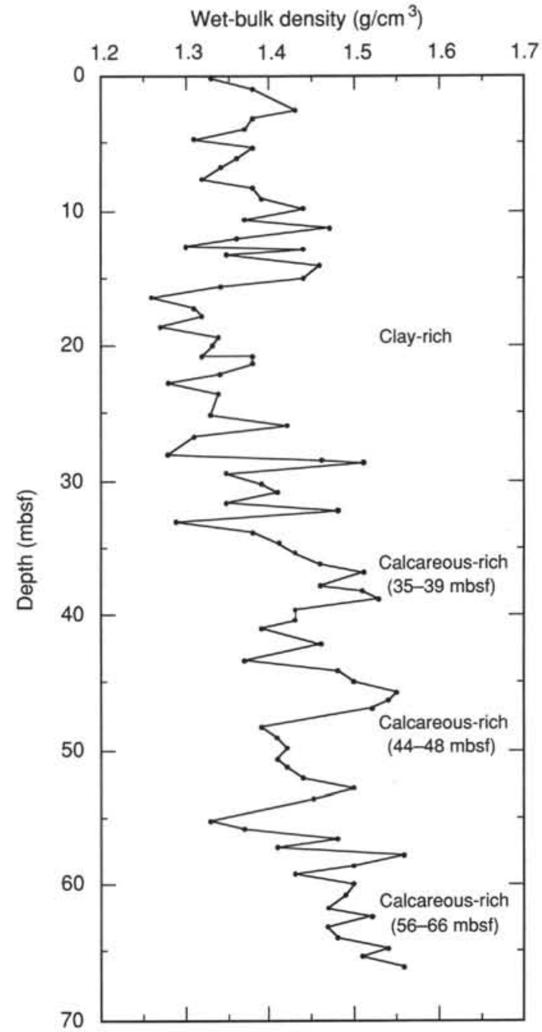

Figure 36. Comparison of wet-bulk density and lithology for Hole 853B.

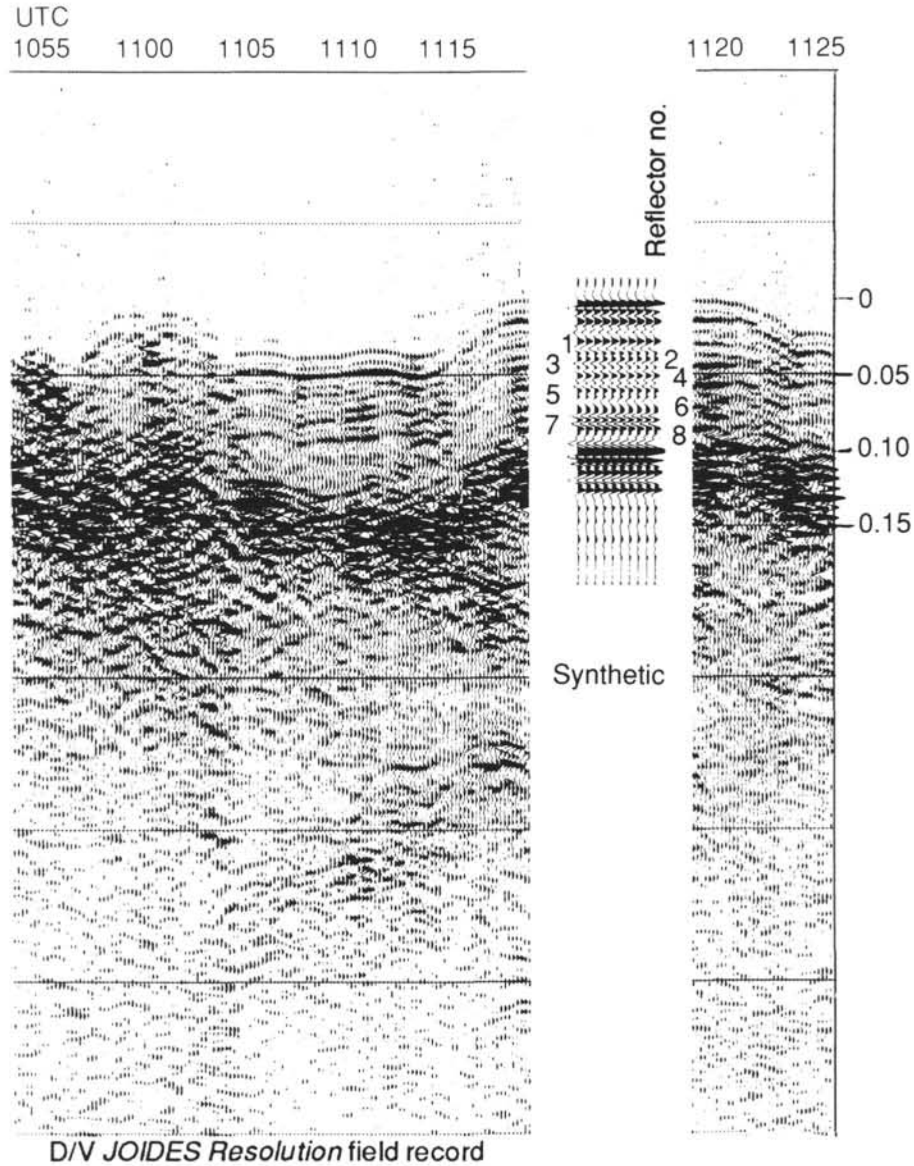

Figure 37. Comparison of synthetic seismogram with field record, Site 853.

Table 17. Summary of traveltimes, depths, and ages for Site 853 reflectors.

Reflector	Traveltime (s)	Synthetic depth (m)	Depth (mbsf)	Depth (mcd)	Age (Ma)
R1	0.024	18.00	17.70	19.40	3.48
	0.037	20.30	19.90	21.50	3.77
R2	0.032	23.90	25.80	25.20	4.10
	0.039	29.10	29.30	28.70	4.54
R3	0.042	31.40	31.90	33.40	4.93
	0.044	32.80	33.20	34.55	5.02
R4	0.047	35.10	34.40	35.70	5.11
	0.050	37.30	36.00	37.30	5.25
R5	0.057	42.50	38.20	38.80	5.37
	0.062	46.20	42.00	43.90	5.70
R6	0.068	50.80	50.30	52.10	6.34
	0.072	53.80	53.30	55.20	6.58
R7	0.076	56.70	55.60	57.50	6.74
	0.078	58.20	58.30	59.90	6.91
R8	0.082	61.20	61.50	64.40	7.20
	0.085	63.40	63.50	66.50	7.38

Table 18. Backtracked path for Site 853.

Age (Ma)	Latitude (°N)	Longitude (°W)
1	6.95	109.06
2	6.70	108.32
3	6.46	107.58
4	6.22	106.84
5	5.98	106.10
6	5.74	105.36
7	5.51	104.62
8	5.28	103.88
9	5.05	103.13
10	4.83	102.39
11	4.60	101.65
12	4.39	100.90
13	4.17	100.15

Using pole of rotation: 0–12 Ma; 67.0°N, 59.0°W.
Angular velocity: 0.83°/m.y.

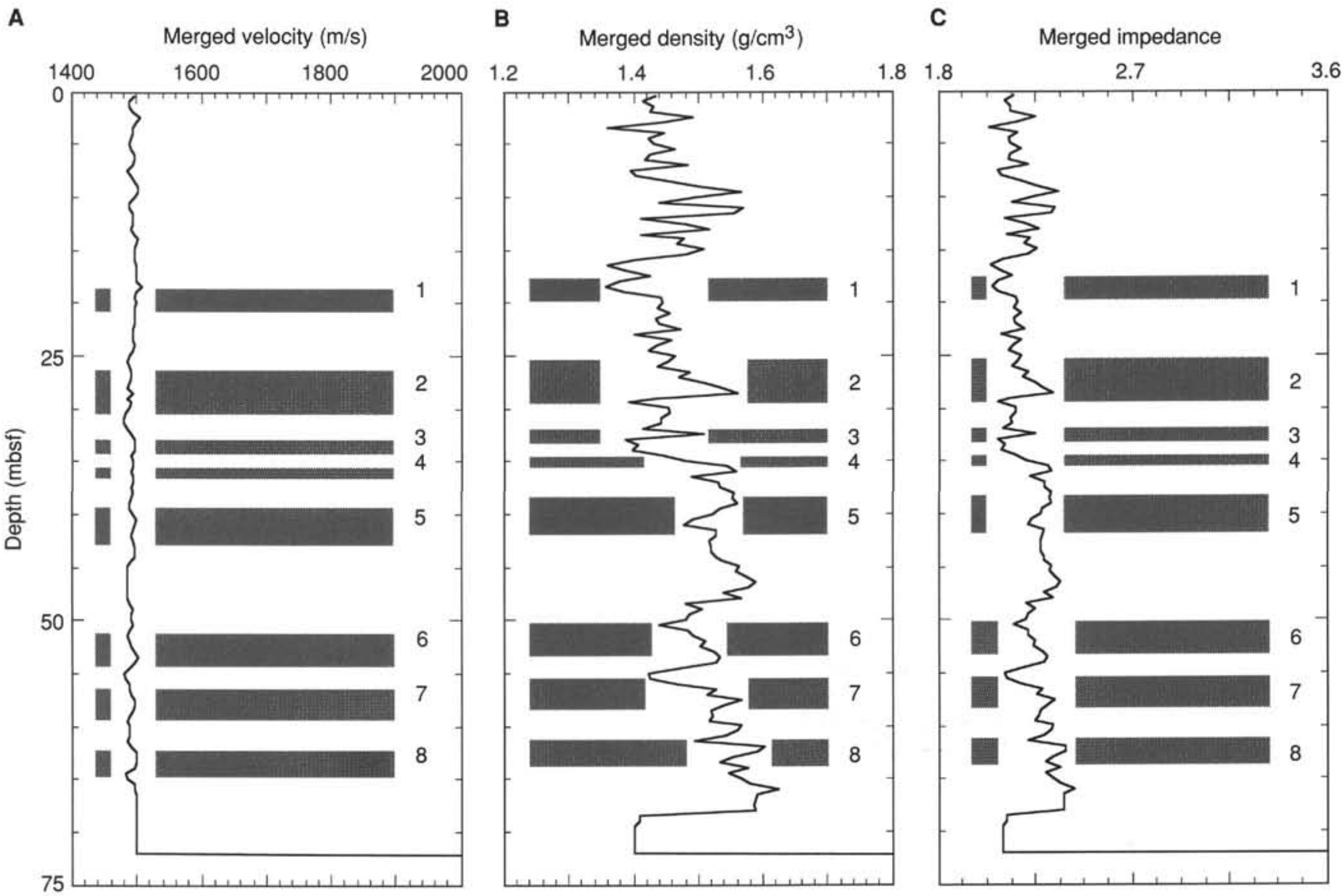

Figure 38. Data used for generating Site 853 synthetic seismograms. **A.** Velocity. **B.** Density. **C.** Acoustic impedance. The 8 reflectors picked from the synthetic seismogram are shown for comparison.

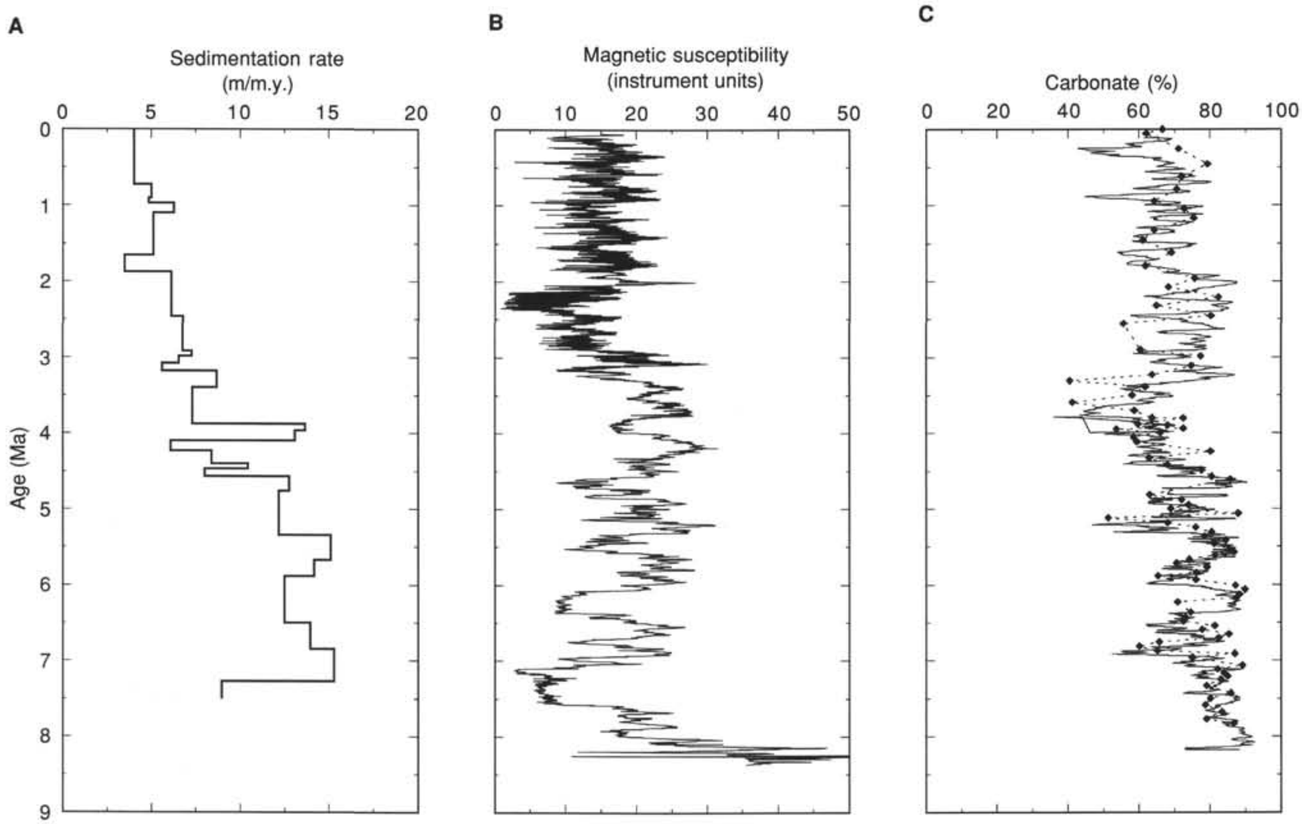

Figure 39. **A.** Sedimentation rate vs. sediment age. **B.** Magnetic susceptibility vs. age. **C.** Predicted (solid line) and measured carbonate content (dashed line with symbol) vs. age.